FUS Regulates Activity of MicroRNA-Mediated Gene Silencing

Graphical Abstract

Highlights

- FUS associates with miRISC components AGO2 and miRNAs and their target transcripts

- FUS is required for optimal miRNA-mediated gene silencing

- *C. elegans* FUS homolog is involved in miRNA-mediated silencing

- ALS-linked FUS R495X mutant impedes miRNA-mediated silencing
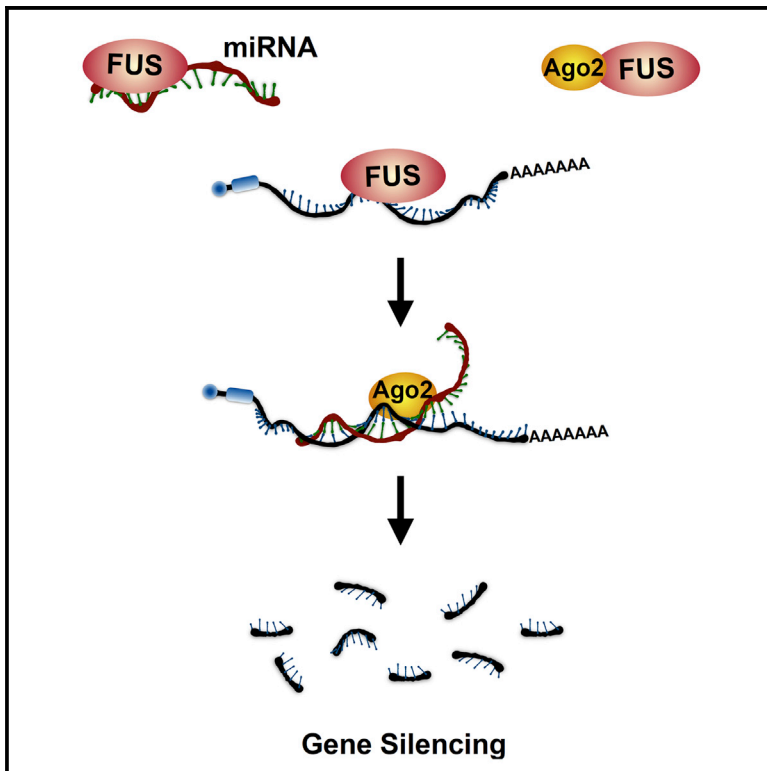
Authors

Tao Zhang, Yen-Ching Wu,
Patrick Mullane, ..., Shao-En Ong,
Anthony K.L. Leung, Jiou Wang

Correspondence

jiouw@jhu.edu

In Brief

Zhang et al. find that the RNA-binding protein FUS is required for miRNA-mediated gene silencing. FUS interacts with Argonaute, microRNAs, and target transcripts, promoting interactions that lead to gene silencing.

Data Resources

GSE68504

CellPress

Cell**Press**

FUS Regulates Activity of MicroRNA-Mediated Gene Silencing

Tao Zhang,[1,2,9] Yen-Ching Wu,[1,2,9] Patrick Mullane,[1,2] Yon Ju Ji,[1,2] Honghe Liu,[1,2] Lu He,[1,2] Amit Arora,[1,2]
Ho-Yon Hwang,[1,2] Amelia F. Alessi,[3] Amirhossein G. Niaki,[4] Goran Periz,[1,2] Lin Guo,[5] Hejia Wang,[5] Elad Elkayam,[6]
Leemor Joshua-Tor,[6] Sua Myong,[4] John K. Kim,[3] James Shorter,[5] Shao-En Ong,[7] Anthony K.L. Leung,[1,8]
and Jiou Wang[1,2,10,*]

[1]Department of Biochemistry and Molecular Biology, Bloomberg School of Public Health, Johns Hopkins University, Baltimore, MD
21205, USA
[2]Department of Neuroscience, School of Medicine, Johns Hopkins University, Baltimore, MD 21205, USA
[3]Department of Biology, Krieger School of Arts and Sciences, Johns Hopkins University, Baltimore, MD 21218, USA
[4]Department of Biophysics, Krieger School of Arts and Sciences, Johns Hopkins University, Baltimore, MD 21218, USA
[5]Department of Biochemistry and Biophysics, Perelman School of Medicine, University of Pennsylvania, Philadelphia, PA 19104, USA
[6]Keck Structural Biology Laboratory, Howard Hughes Medical Institute, Cold Spring Harbor Laboratory, Cold Spring Harbor, NY 11724, USA
[7]Department of Pharmacology, University of Washington, Seattle, WA 98195, USA
[8]Department of Oncology, School of Medicine, Johns Hopkins University, Baltimore, MD 21205, USA
[9]These authors contributed equally
[10]Lead Contact
*Correspondence: jiouw@jhu.edu
https://doi.org/10.1016/j.molcel.2018.02.001

SUMMARY

MicroRNA-mediated gene silencing is a fundamental mechanism in the regulation of gene expression. It remains unclear how the efficiency of RNA silencing could be influenced by RNA-binding proteins associated with the microRNA-induced silencing complex (miRISC). Here we report that fused in sarcoma (FUS), an RNA-binding protein linked to neurodegenerative diseases including amyotrophic lateral sclerosis (ALS), interacts with the core miRISC component AGO2 and is required for optimal microRNA-mediated gene silencing. FUS promotes gene silencing by binding to microRNA and mRNA targets, as illustrated by its action on miR-200c and its target *ZEB1*. A truncated mutant form of FUS that leads its carriers to an aggressive form of ALS, R495X, impairs microRNA-mediated gene silencing. The *C. elegans* homolog *fust-1* also shares a conserved role in regulating the microRNA pathway. Collectively, our results suggest a role for FUS in regulating the activity of microRNA-mediated silencing.

INTRODUCTION

RNA-binding proteins (RBPs) play important roles in the regulation of gene expression and the development of human diseases. Amyotrophic lateral sclerosis (ALS) is a devastating progressive neurodegenerative disorder characterized by loss of motor neurons. Over 40 mutations in FUS have been linked to 4% of ALS cases, including both familial and sporadic forms (Kwiatkowski et al., 2009; Vance et al., 2009). FUS proteinop-

athy is a common feature in ALS (Deng et al., 2010) and is also present in patients with frontal temporal lobar degeneration, the second most common dementia that afflicts individuals under the age of 65 (Mackenzie et al., 2010). While FUS normally shuttles between the nucleus and cytoplasm, a large proportion of ALS-associated FUS mutations localize to its C-terminal nuclear localization sequence (NLS), resulting in its impaired nuclear transport (Bosco et al., 2010; Dormann et al., 2010; Gal et al., 2011; Ito et al., 2011; Lanson et al., 2011). A truncated mutant form of FUS, R495X, that lacks the last 32 amino acids containing the NLS, causes patients to exhibit an earlier onset of ALS with more severe symptoms than those with other missense mutations (Waibel et al., 2013). However, how the disease mutations affect the functions of FUS is not fully understood.

FUS is a DNA/RNA-binding protein containing an N-terminal serine-tyrosine-glycine-glutamine (SYGQ)-rich region, a glycine-rich (G-rich) region, a central conserved RNA recognition motif (RRM), and a zinc-finger motif (ZNF) that is flanked by C-terminal arginine-glycine-glycine (RGG) boxes. FUS binds RNA through its RRM, ZNF, and RGG domains (Iko et al., 2004; Prasad et al., 1994) and has a wide range of RNA-binding abilities (Wang et al., 2015), including the recognition of a GGUG motif (Lerga et al., 2001) and AU-rich stem-loop structures (Hoell et al., 2011). FUS is involved in multiple cellular processes, including the maintenance of genomic integrity (Mastrocola et al., 2013; Qiu et al., 2014; Wang et al., 2013), transcription (Schwartz et al., 2012; Tan and Manley, 2010; Uranishi et al., 2001; Yang et al., 2014), pre-mRNA splicing (Dichmann and Harland, 2012; Lagier-Tourenne et al., 2012; Sun et al., 2015; Zhou et al., 2013), and alternative polyadenylation (Masuda et al., 2015). FUS was reported to be involved in the biogenesis of microRNA (miRNA) by recruiting Drosha to pri-miRNAs at their transcription sites and contributes to the biogenesis of a subset
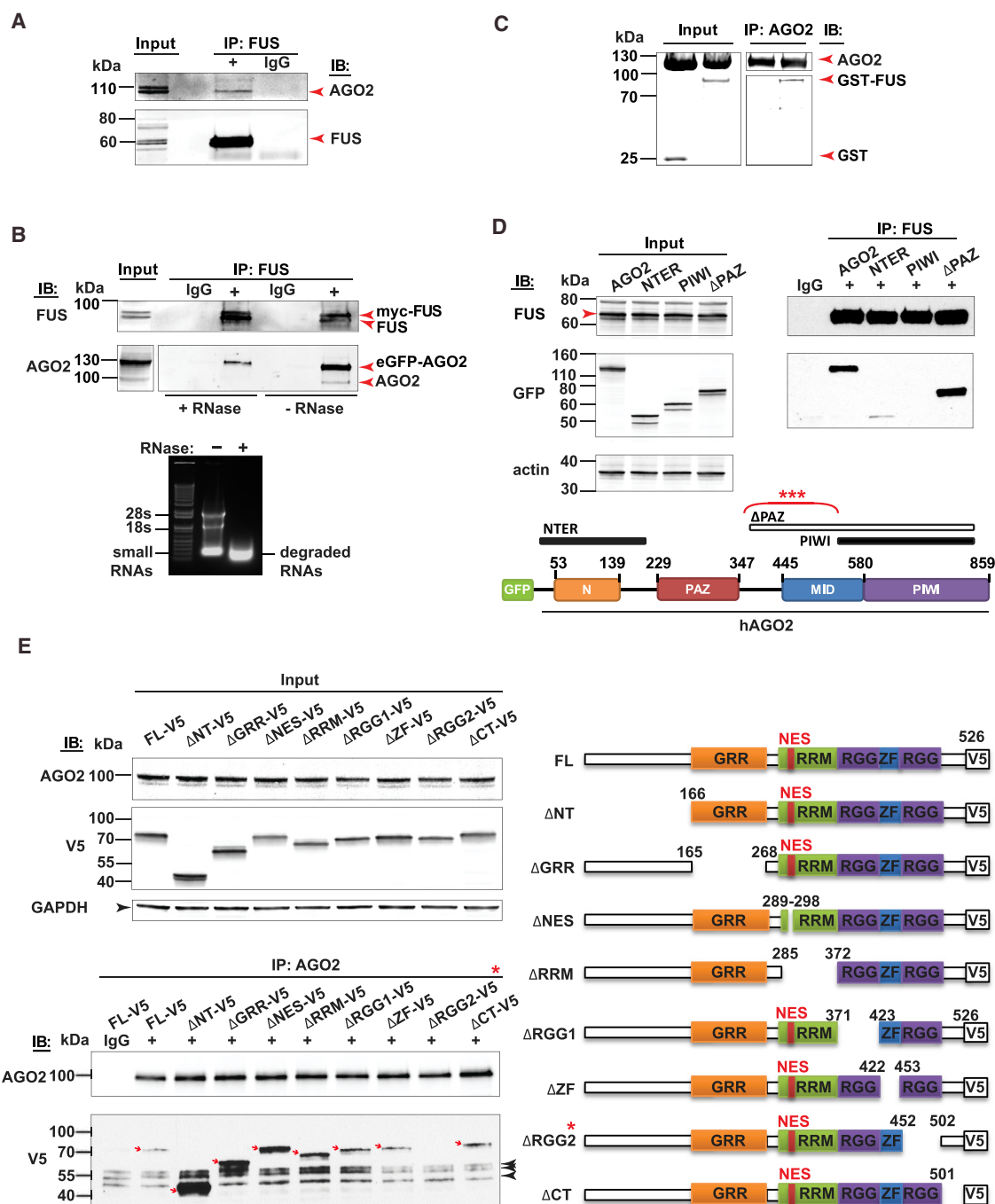
Figure 1. FUS Interacts with AGO2

(A) Immunoblots of a coIP experiment conducted in mouse forebrain lysates where FUS IP pulled down endogenous AGO2. Red arrows indicate the protein bands for FUS and AGO2.

(B) Immunoblots of coIP experiments conducted in HEK293 cell lysates expressing eGFP-AGO2 and myc-FUS where FUS IP pulled down recombinant and endogenous AGO2 in the presence and absence of RNase A treatment. Red arrows distinguish between recombinant and endogenous forms of AGO2 and FUS. Shown below the immunoblots is an agarose gel loaded with the total RNAs enriched with small RNA fractions from HEK293 cells that were treated with or without RNase A in parallel to the coIP experiments, demonstrating that most RNAs are degraded into short fragments.

(C) Direct interaction between GST-FUS and AGO2. Left: the inputs of purified AGO2, GST-FUS, and GST proteins were shown on SDS-PAGE by Coomassie blue stain. Right: the coIP immunoblots were shown with AGO2 as the bait and the pulled GST-FUS detected by an anti-GST antibody.

(D) Immunoblots of FUS coIP experiments conducted in HEK293 cells that expressed various eGFP-tagged WT or truncation AGO2 mutants. The red arrow points to the FUS protein band. A graphical depiction of the AGO2 truncation mutants is illustrated below with the presence (white) or absence (black) of

(legend continued on next page)

of miRNAs (Morlando et al., 2012). However, it remains unknown if FUS plays a direct role in the regulation of the function of mature miRNAs.

miRNAs are small non-coding single-stranded RNAs, containing ~22 nucleotides that post-transcriptionally regulate gene expression of most human coding mRNAs. In mammals, miRNAs are initially derived from primary pri-miRNAs synthesized by RNA polymerase II, which are further processed into an miRNA duplex by two RNase III enzymes: Drosha and Dicer. One strand of the duplex then loads onto one of four Argonaute (AGO) proteins, forming the core of miRNA-induced silencing complex (miRISC). This complex then binds to TNRC6A (GW182) to repress translation and accelerate decay of mRNA targets. The miRNA-mRNA pairing is mediated by a 6–8 nucleotide short seed region, and miRISC utilizes the guide strand to target mRNAs by Watson-Crick base pairing to partial complementary sequences within their 3′ UTRs or coding regions. It is considered a major challenge for miRISC to locate the target mRNAs with high efficiency and specificity (Herzog and Ameres, 2015), and it remains unknown if there are other players that facilitate AGOs in miRNA target recognition. The regulation of gene expression by miRNAs can be altered positively or negatively by RBPs associated with the target mRNAs (Bhattacharyya et al., 2006; Kedde et al., 2007; Vasudevan et al., 2007). Recent data suggest that the miRNA regulation could be more complex than previously thought—only a small fraction (<10%) of miRNAs are AGO bound (Janas et al., 2012; Stalder et al., 2013) and miRNAs exist in high excess relative to AGOs (Janas et al., 2012). Furthermore, certain miRNAs directly bind proteins (Leung, 2015), such as AUF1, which promotes miRNA loading on AGO2 (Yoon et al., 2015). The significance and prevalence of the phenomenon of direct protein binding to specific miRNAs remain unclear. Here we report findings that FUS is required for optimal gene silencing mediated by mature miRNAs through its association with miRISC components.

RESULTS

FUS Interacts with Argonaute 2

We identified FUS in two independent protein interaction screens using eGFP-tagged or HA-tagged AGO2 as bait (Table S1). We confirmed this interaction by immunoprecipitation (IP) of FUS from adult male c57bl6 mouse forebrain lysates and detection of endogenous AGO2 in the immunoprecipitates (Figure 1A). Conversely, we confirmed the endogenous interaction by IP of AGO2 and detection of FUS in mouse embryonic fibroblast (MEF) cells (Figure S1A). Since FUS and AGO2 are both RBPs, we asked whether their association is RNA dependent. To test for RNA dependency, we expressed myc-FUS and eGFP-AGO2 in HEK293 cells, performed IP of FUS, and

treated one half of the immunoprecipitate with excess RNase A while leaving the other half untreated. The amount of AGO2 present in the FUS immunoprecipitate decreased substantially after the RNase A treatment, although this loss was not complete (Figure 1B). Furthermore, the endogenous interaction of AGO2 and FUS was also substantially decreased after the RNase A treatment (Figure S1A). Therefore, FUS association with AGO2 is mainly RNA dependent.

To test whether AGO2 and FUS can interact directly, we purified human AGO2 protein and GST-tagged human FUS protein and demonstrated through coIP that AGO2 can pull down GST-FUS, but not a GST control, indicating a direct interaction between AGO2 and FUS in vitro (Figure 1C). To further confirm interaction between FUS and AGO2, we found that a subset of endogenous FUS and endogenous AGO2 co-localized in cytoplasmic granules in HeLa cells (Figure S1B). Since there are eight AGO family members, we tested whether the interaction between FUS and AGO2 is unique to AGO2. We confirmed an interaction between FUS and AGO1 by IP (Figure S1C).

To identify the region in AGO2 that mediates its association with FUS, we conducted a series of coIP experiments in HEK293 cells expressing various eGFP-tagged forms of AGO2, including wild-type (WT) and truncation mutants (NTER, ΔPAZ, and PIWI) (Figure 1D). While the NTER and PIWI AGO2 truncation mutants exhibited reduced association with FUS, such an effect was absent with the ΔPAZ truncation mutant. Since only the ΔPAZ mutant contains the MID (middle) domain of AGO2, our coIP data indicate that the MID domain of AGO2 is critical for FUS binding. We also conducted a series of reverse coIPs in HEK293 cells that expressed V5-tagged WT or other truncated forms of FUS to identify regions of FUS that mediate its binding to AGO2. We determined that the RGG2 domain of FUS is needed for its association with endogenous AGO2, since only the mutant that lacked this region of FUS (ΔRGG2-V5) exhibited loss of binding to AGO2 (Figure 1E).

FUS Promotes Mature miRNA-Mediated Gene Silencing

Having observed an interaction between FUS and AGO2, we probed whether FUS plays a role in mature miRNA-mediated gene silencing. To address whether loss of FUS would have any effect on miRNA silencing, we obtained a mouse strain that harbors an FUS deletion allele that lacks all of its exons (Figure 2A). We observed viable heterozygous $FUS^{+/-}$ mice, but were unable to find any postnatal homozygous $FUS^{-/-}$ mice, indicative of their prenatal lethality. However, we found viable $FUS^{-/-}$ mice on embryonic day 12, and therefore generated MEF cells. To directly probe a potential role for FUS in the mature miRNA-mediated gene silencing, we used an miRNA activity reporter in which the 3′ UTR of Renilla reniformis luciferase (RL) harbors six bulged binding sites for a small interfering RNA

associations between recombinant AGO2 and endogenous FUS noted. Red asterisks highlight the MID region of AGO2 as important for mediating its interaction with FUS.

(E) Left: immunoblots of endogenous AGO2 coIP experiments conducted in HEK293 cells that expressed recombinant C-terminally V5-tagged WT or truncated mutant FUS proteins. Triple black arrows directed at the V5 IP blot indicate non-specific bands recognized by the V5-HRP antibody used to detect the recombinant FUS proteins. Right: schematic of the graphical depictions of the FUS-V5 tagged constructs. Red asterisks indicate the only FUS mutant that does not associate with endogenous AGO2. In all coIP experiments, a species-matched IgG-isotype antibody served as the IP control.

See also Figure S1 and Table S1.
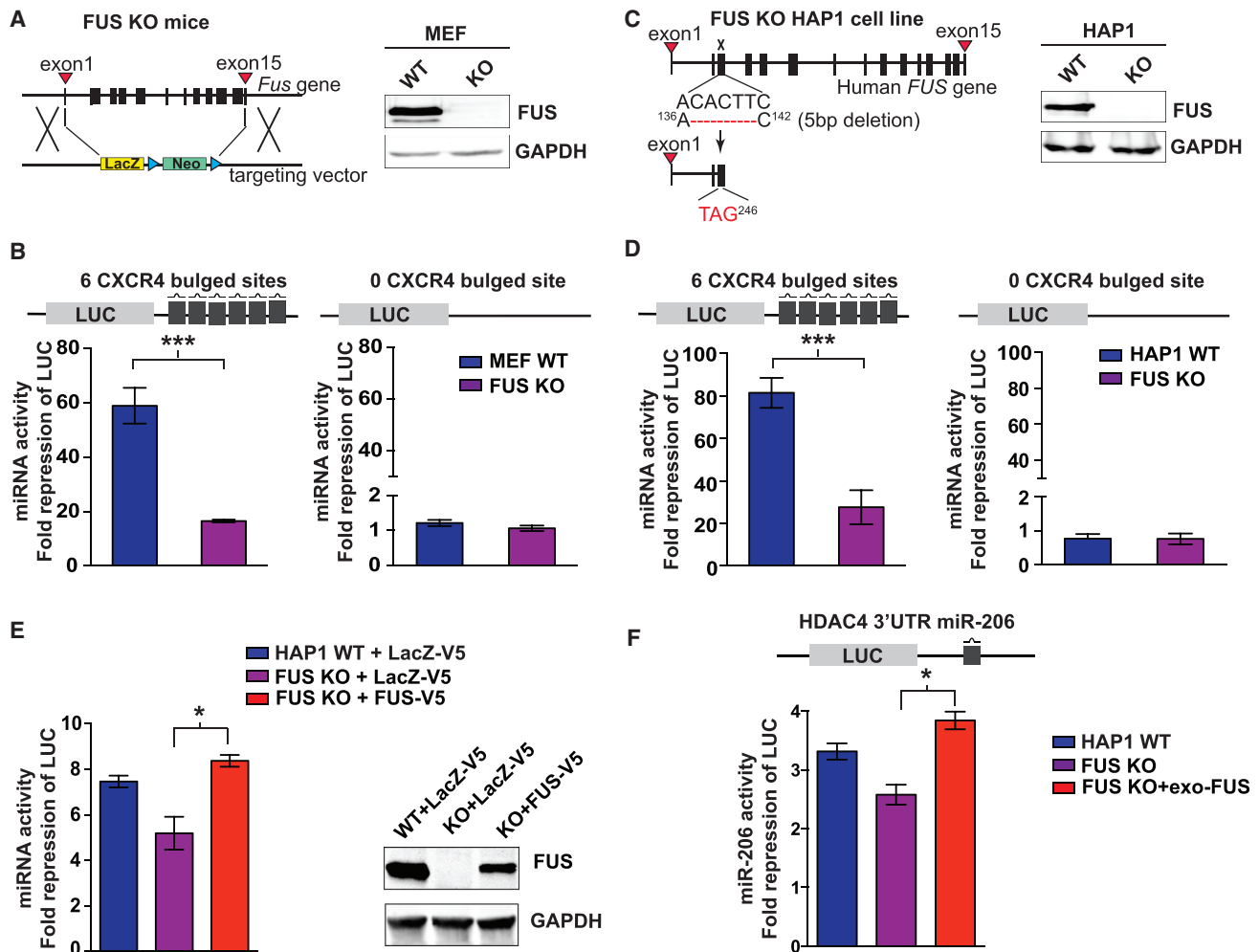
Figure 2. FUS Is Required for Optimal Mature miRNA-Mediated Silencing

(A) Left: schematic of the deletion allele in the FUS KO mice. Right: immunoblots of the endogenous FUS and GAPDH in FUS WT and KO MEF cell lines.

(B) Bar graph represents fold repression of *Renilla* luciferase reporters that contain six imperfect bulge target sites (pRL-6X) or no sites (pRCP-0P) for siCXCR4, which were co-transfected with the normalization control pGL3 firefly reporter in FUS WT and KO MEF cells (n = 3).

(C) Left: schematic of the human FUS KO allele, which was engineered by CRISPR/Cas9 genome editing to produce a 5 bp deletion that results in a premature stop codon in exon 3. Right: immunoblots of the endogenous FUS and GAPDH conducted in human FUS WT and KO HAP1 cell lines.

(D) Bar graph represents fold repression of pRL-6X or pRCP-0P for siCXCR4 in human FUS WT and KO HAP1 cells (n = 3) as in (B).

(E) Left: bar graph represents fold repression of pRL-6X for siCXCR4 in HAP1 WT or FUS KO cells, which were co-transfected with V5-tagged FUS or LacZ. The exogenous FUS, but not LacZ, rescued the silencing defect of the FUS KO cells (n = 3). Right: immunoblots of FUS in HAP1 WT or FUS KO cells.

(F) Bar graph represents fold repression of the Pp-WT-HDAC4 reporter by miR-206 that were co-transfected into HAP1 WT or FUS KO cells with the latter being rescued by an exogenous FUS construct. Fold repression is calculated by normalizing the firefly luciferase activity against the *Renilla* activity of the pRCP-0P (n = 3). Error bars represent ± SEM. *p ≤ 0.05, ***p ≤ 0.001.

See also Figure S1.

(siRNA), siCXCR4, mimicking the mode of a typical miRNA binding (Leung et al., 2011). This reporter system bypasses the miRNA biogenesis steps and provides a sensitive measurement for mature miRNA activities and the efficiency of gene silencing. To calculate the fold repression exerted by siCXCR4, the level of luciferase activity in the presence of siCXCR4 is normalized against the activity in the presence of a negative control siRNA, which has no homology to any known mammalian genes. When the reporter system was tested in WT MEFs, siCXCR4 repressed the luciferase reporter activity more greatly than the control

siRNA as expected. However, in FUS knockout (KO) MEFs, the silencing activity of siCXCR4 was significantly reduced, indicating that the loss of FUS resulted in impairment in CXCR4's silencing activity (Figure 2B, left). When the CXCR4 target sites were removed from the luciferase reporter, this differential effect between the WT and KO MEFs on silencing was abolished (Figure 2B, right), confirming the specificity of the observed effects of FUS on miRNA activity. Furthermore, we examined the miRNA-mediated gene silencing in a human FUS KO cell line generated from haploid HAP1 cells (Figure 2C). Using the
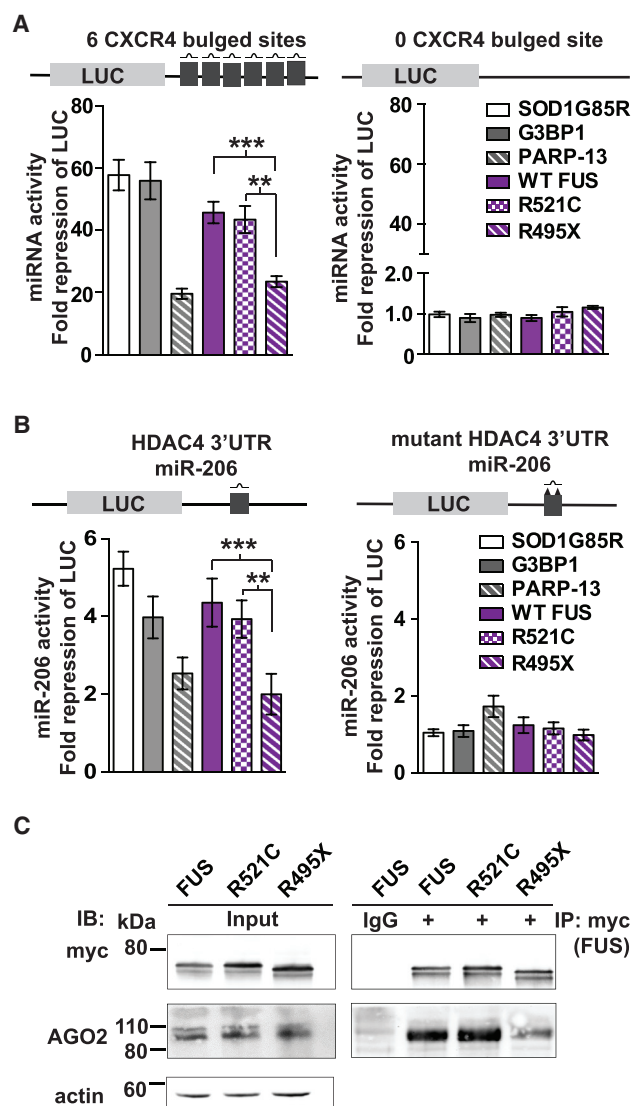
Figure 3. ALS-Associated FUS Truncation Mutant R495X Interferes with miRNA-Mediated Silencing Activity

(A) Bar graph represents fold repression of *Renilla* luciferase reporters that contain six imperfect bulge target sites (pRL-6X) or no sites (pRCP-0P) for siCXCR4, which were co-transfected with the normalization control pGL3 firefly reporter along with myc-FUS, myc-R521C, myc-R495X, myc-SOD1G85R, eGFP-G3BP1, or eGFP-PARP-13 in HEK293 cells. Fold repression is measured by taking the normalized *Renilla* luciferase activity in cells treated with the control siRNA divided by the value in cells treated with the active CXCR4 siRNA (n = 5). (B) Bar graph represents fold repression of the Pp-WT-HDAC4 reporter or the mutant Pp-Mt-HDAC4 reporter that was co-transfected in HEK293 cells with the normalization control pRCP-0p *Renilla* reporter, in addition to the same myc- or eGFP-tagged constructs as in (A). Fold repression is calculated similarly as in (A) except that firefly luciferase activity is normalized against the *Renilla* activity of the pRCP-0P and that miR-206 replaces CXCR4 siRNA (n = 4). (C) R495X exhibits weakened association with AGO2. Immunoblots of myc immunoprecipitates from HEK293 cell lysates that were co-transfected with myc-FUS, myc-R521C, or myc-R495X, which were subsequently probed for endogenous AGO2. A species-matched IgG-isotype antibody served as the IP control. One-way repeated ANOVA is used for statistics. Error bars represent ± SEM. **$p \leq 0.01$, ***$p \leq 0.001$.
See also Figure S1.

siCXCR4 reporter system, we found that the FUS KO HAP1 cells also exhibited a defect in the miRNA activity. Relative to control HAP1 cells, FUS KO cells showed greater than a 3-fold reduction in siCXCR4 silencing activity (Figure 2D). Next, we tested whether the reduced miRNA-mediated gene silencing effect caused by loss of FUS would be rescued by exogenous FUS. In HAP1 FUS KO cells, the expression of V5-tagged FUS, but not a LacZ-V5 control, reversed the deficits in the miRNA activity caused by loss of endogenous FUS as measured by the siCXCR4 reporter system (Figure 2E).

Next, we evaluated the activity of miR-206, an miRNA previously demonstrated to slow ALS progression and promote regeneration of neuromuscular synapses through translational repression of its target histone deacetylase 4 (HDAC4) in mice (Williams et al., 2009). We utilized a luciferase reporter containing the WT HDAC4 3′ UTR with the miR-206-binding site and observed that the activity of mature miR-206 was significantly reduced by the deletion of FUS in HAP1 cells, a defect rescued by the introduction of exogenous FUS (Figure 2F). Additionally, using an siRNA oligonucleotide that was perfectly complementary to a segment of the HDAC4 3′ UTR reporter, a similar defect in the silencing activity upon loss of FUS was observed (Figure S1H). Together, these results indicate that endogenous FUS is required for mature miRNA-mediated gene silencing in mammalian cells.

ALS-Associated Mutation R495X Interferes with miRNA Activity

We asked whether ALS-linked mutation in FUS would affect miRNA-mediated gene silencing (Figure 3A). Using the miRNA activity assay, we co-expressed myc-tagged WT FUS, the ALS-associated FUS point mutant R521C, the ALS-associated FUS truncation mutant R495X, or an ALS-associated mutant form of superoxide dismutase 1 (SOD1G85R) with the siCXCR4 luciferase reporter system into HEK293 cells. We used Ras GTPase-activating protein-binding protein 1 (G3BP1) and poly(ADP-ribose) polymerase 13 (PARP-13) as a negative and a positive control, respectively (Leung et al., 2011). Compared with G3BP1, the mutant SOD1G85R, myc-tagged WT FUS, or point mutant R521C did not significantly alter the miRNA activity of siCXCR4. In contrast, the truncated mutant R495X significantly reduced silencing to a similar degree as the positive control PARP-13—an effect that was absent when no CXCR4 target site was present (Figures 3A and S1D), demonstrating that the inhibitory effect of R495X is specific to the recognition of the reporter mRNA by siCXCR4.

Next, we examined whether R495X disrupts the silencing of the miR206-HDAC4 pair. We utilized the luciferase reporters containing either a WT HDAC4 3′ UTR or a mutant that carries two point mutations in the miR-206-binding site (Figure 3B) and examined the effect of FUS and its mutants, as in Figure 3A. Consistent with the effects observed with the siCXCR4 system, only R495X expression significantly reduced miR-206-mediated silencing of the WT HDAC4 reporter, an effect that was absent when the miR-206-binding site was mutated in the HDAC4 3′ UTR reporter (Figures 3B and S1E). Together, since the miRNA activity reporters rely on exogenous siCXCR4 or miR-206 and bypass the miRNA biogenesis steps, these data indicate that

R495X can interfere with mature miRNA-mediated silencing in the cell.

Next, we investigated whether the reduced silencing by R495X reflected changes to its association with AGO2, as this truncated mutant lacks a portion of FUS RGG2 domain, which we identified as being important for mediating FUS association with AGO2 (Figure 1E). To test this hypothesis, we immunoprecipitated myc-tagged proteins from HEK293 cells expressing myc-FUS, myc-R521C, or myc-R495X and probed for endogenous AGO2 (Figure 3C). Compared with WT FUS, the mutant R495X, but not R521C, bound less endogenous AGO2 protein. The reduced interaction between R495X and AGO2 also occurred when both AGO2 and R495X were co-expressed in HEK293 cells (Figures S1F and S1G). Thus, the absence of a portion of the RGG2 domain in R495X results in a reduced association between FUS and AGO2, a defect that likely underlies the impaired silencing effect that was observed following exogenous expression of R495X (Figure 3).

Transcriptome Profiles Reveal Specific FUS-Dependent miRNA Silencing

We performed transcriptome analyses using both mRNA and miRNA microarrays in parallel, with RNA extracted from HEK293 cells expressing either myc-tagged WT FUS or R495X. Among the differentially regulated mRNAs (Table S2), we confirmed the expression changes in a subset of genes related to neural development and disease (Figures 4A and 4B). Among the differentially regulated miRNAs (Table S3), miR-200c was most significantly regulated (Figure 4C). As confirmed by qPCR, miR-200c levels were lower in R495X-expressing cells compared with WT FUS-expressing HEK293 cells (Figure 4D). The difference in the mature miR-200c levels could be in part due to the lower levels of the precursor pri-miR-200c in R495X-expressing cells (Figure S1I). Consistent with the recent report that FUS promotes the biogenesis of miR-200c (Morlando et al., 2012), we confirmed that FUS interacted with Drosha but R495X mutant showed reduced association with the protein in coIP experiments (Figure S1J). Since miR-200c and its target transcript ZEB1 are an miRNA-mRNA pair conserved between human and mice, we analyzed their levels in mouse motor neurons after transduction with WT or R495X FUS. As expected, WT FUS increased the level of miR-200c and decreased the level of the ZEB1 mRNA (Figure S2B). However, compared with WT FUS, R495X-expressing cells had a lower level of miR-200c and failed to induce the silencing of ZEB1, indicating that R495X caused dysregulation of miR-200c and ZEB1 expression in neurons. To confirm that the effects of FUS on ZEB1 mRNA were dependent on miR-200c, we inhibited miR-200c activity by applying a sequence-specific antagomir, which abolished the differential regulation of ZEB1 mRNA levels by WT FUS and R495X in HEK293 cells (Figure S2C), indicating that FUS acts through miR-200c to influence ZEB1 transcript levels.

The most interesting observation from our combined mRNA and miRNA microarray datasets is not the changes in the levels of miRNAs but the direction of changes in the levels of mRNA targets of most miRNAs. While cross-referencing the miRNA and mRNA transcript datasets, we observed a highly significant trend of an enrichment of upregulated mRNA targets for the majority of miRNAs (Figure 4E). Among the most significantly regulated mRNA transcripts ([fold change] > 2, false discovery rate [FDR] < 0.05) (Table S4), we counted the number of up- versus downregulated mRNA targets for each miRNA family, and observed that the majority of the miRNAs have significantly more upregulated mRNA targets than downregulated targets in the presence of R495X (Figure 4E; Table S4). This trend is independent of the direction of changes in miRNA levels, suggesting that it is the activity, rather than the biogenesis, of miRNAs that drives the changes in mRNA target expressions. Next, we identified a set of representative miRNA-mRNA pairs, in which the miRNA levels are not decreased but their target mRNA levels are significantly upregulated ([fold change] > 2, FDR < 0.05) in R495X-expressing cells. Among them, we selected mRNAs that are FUS targets and harbor FUS-binding sites in their 3' UTRs based on previous PAR-CLIP data (Hoell et al., 2011). qRT-PCR analysis validated that the levels of both these miRNAs and mRNAs are increased in R495X-expressing cells (Figure 4F). In addition, R495X increases the levels of HDAC4 mRNA despite the increase of the matching miR-206 (Figure 4F), in line with the results that R495X impairs the miRNA activities (Figure 3). As a negative control, we measured the levels of several mRNAs that were validated targets of non- or low-expressing miRNAs in HEK293 cells. The lack of upregulation of these mRNAs in R495X-expressing cells suggests that they are not regulated by FUS-dependent miRNA silencing pathways (Figure S2D). Together, the observation that most of the target mRNAs are upregulated even when the corresponding miRNAs are upregulated supports the notion that R495X may have affected mature miRNA activities.

Further analyses cross-referencing our microarray data with CLIP-seq (crosslinking immunoprecipitation sequencing) data on FUS and AGO2 binding targets (Hoell et al., 2011; Kishore et al., 2011) suggest that FUS plays a role in regulating miRNA activity. First, there is a substantial overlap between FUS and AGO2 3' UTR targets, with 85% of FUS targets bound by AGO2 and 44% of AGO2 targets bound by FUS (Figure S2E). We further observed that FUS and AGO2 are proximately localized at the 3' UTRs of most of their shared targets (Figure S2F). In addition, FUS targets that are differentially regulated upon expressing R495X tend to have long 3' UTRs—a feature shared with miRNA targets (Bartel, 2009) (Figures S2G and S2H). Furthermore, we observed a highly significant correlation between FUS-binding RNA targets and the regulated transcripts in the microarray: AGO2 binds the majority of genes that are upregulated in R495X-expressing cells but only a minority of downregulated genes, while the majority of non-FUS target genes are downregulated (Figure S2I). Similarly, FUS targets that are differentially regulated in R495X-expressing cells tend to be upregulated (Figure S2I). When the most significantly regulated mRNA transcripts ([fold change]>2, FDR < 0.05) are analyzed, the trend is even more pronounced: AGO2 or FUS targets were more significantly enriched for upregulated mRNAs than for downregulated mRNAs (Figure S2J).
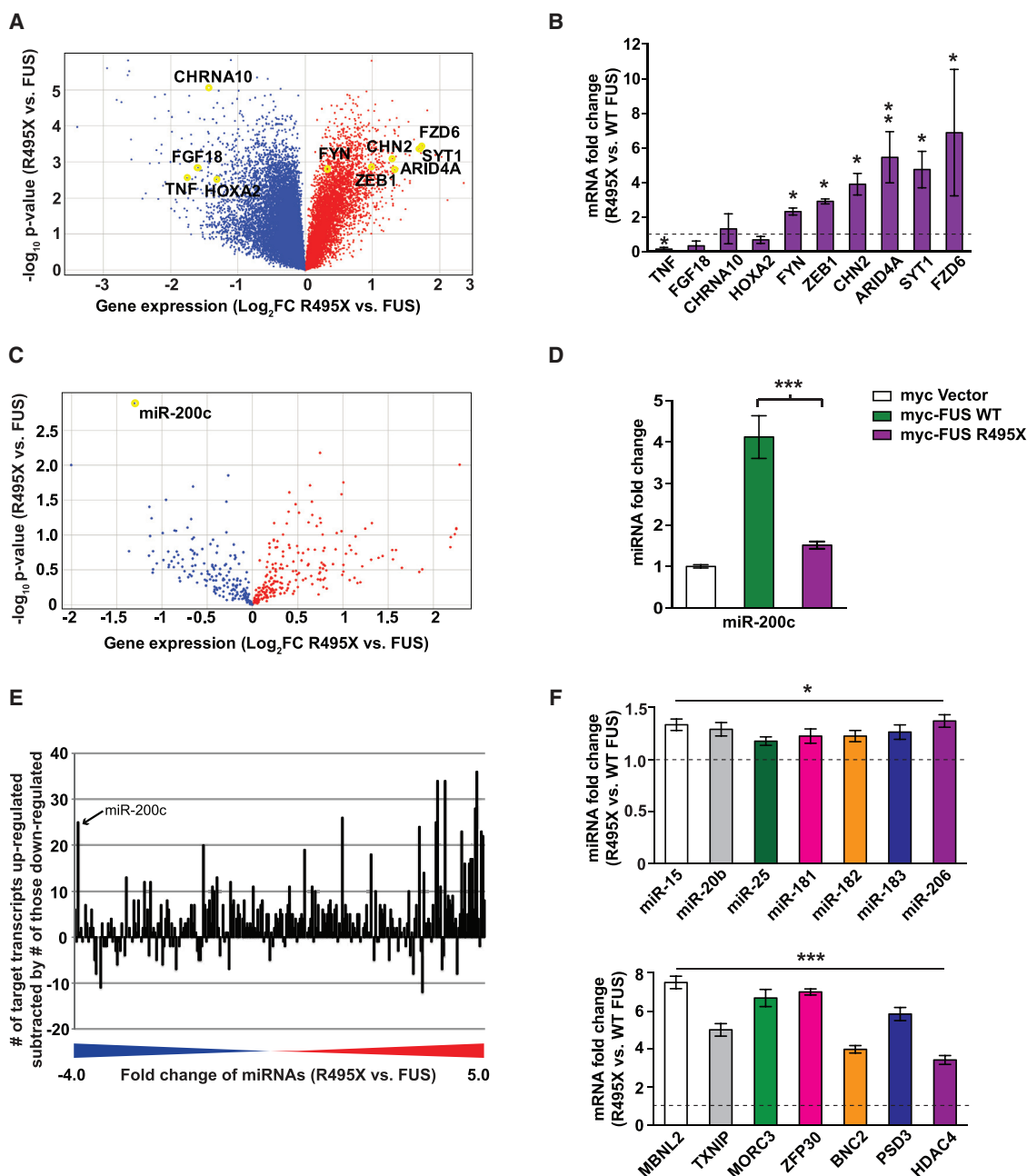
Figure 4. ALS-Linked R495X Mutant FUS Alters the Expression of miRNA Target Transcripts Globally

(A) A volcano plot of the exon microarray results, in which mRNA transcripts that are up- (red) or downregulated (blue) in cells that express myc-R495x versus myc-FUS are represented with the p value as a function of the fold change (FC). Highlighted in yellow are a subset of genes related to neural development and disease.

(B) Bar graph represents the relative expression levels of representative mRNA transcripts as confirmed by qPCR (n = 3). The ratios of R495X to WT FUS levels are shown.

(C) A volcano plot of the miRNA microarray results, in which miRNAs that are up- (red) or downregulated (blue) in cells that express myc-R495X versus myc-FUS are represented with the p value as a function of the fold change. Highlighted in yellow is miR-200c.

(D) Bar graph represents the expression levels of mature miR-200c as confirmed by qPCR (n = 6).

(E) A global trend of upregulation of miRNA-targeted mRNA transcripts. Analysis of all the miRNAs with matched target mRNAs that are significantly regulated ([fold change] > 2, FDR < 0.05). y axis is the number of upregulated target mRNAs subtracted by the number of downregulated mRNAs in the presence of R495X. x axis is the fold change of the miRNAs. The enrichment of upregulated target transcripts is highly significant (p < 0.001, two-way paired ANOVA).

(F) Bar graph represents the relative expression levels of representative miRNA-mRNA pairs (marked by matching colors), as measured by qPCR (n = 3). Error bars represent ± SEM. *p ≤ 0.05, **p ≤ 0.01, ***p ≤ 0.001.

See also Figures S1 and S2 and Tables S2, S3, and S4.

C. elegans Homolog of FUS Plays a Role in the miRNA Pathway

C. elegans has a homolog of human FUS, FUST-1, that shares ~47% similarity in amino acid sequence composition and contains both the RRM and ZNF motifs. We asked how loss of *fust-1* might affect the miRNA pathways in miRNA-sensitized genetic backgrounds. *C. elegans* has >26 Argonaute genes, including *alg-1* and *alg-2*, both of which are required for miRNA activities (Yigit et al., 2006). *C. elegans* with the loss-of-function allele of *alg-1*(*gk214*) have phenotypes of incomplete alae formation and vulva bursting or "bag of worms" due to the heterochronic developmental defects in seam cells and vulva, respectively (Grishok et al., 2001). We crossed a *fust-1* deletion mutant, *tm4439*, to *alg-1*(*gk214*) and observed strong synergistic effects on the vulva and alae phenotypes in the *fust-1;alg-1* double mutant. The loss-of-function *fust-1* (*tm4439*) allele significantly enhanced the vulva development defect in *alg-1*(*gk214*), as scored by vulva bursting and worm bags in adults 3 days after the fourth larval stage, L4, at 20°C (Figure 5A). Moreover, *fust-1*(*tm4439*) allele enhanced the alae development defect in *alg-1*(*gk214*), as quantified by counting animals with incomplete alae formation 16 hr after L4 at 20°C (Figure 5B). The incomplete formation of alae in the mutants was consistent with the extra division of seam cells, as quantified by counting the number of seam cells on both left and right sides of the body at the L4 stage at 20°C (Figures 5C and S3A). Accordingly, the heterochronic gene *lin-41*, whose stage-dependent silencing is critical for normal vulva and alae development, was upregulated in the *fust-1;alg-1* double mutant compared with the single mutant (Figure S3B). Since *lin-41* is a target of the *let-7* miRNA (Reinhart et al., 2000), we asked whether *fust-1* influenced the *let-7* activity by crossing *fust-1*(*tm4439*) into a hypomorphic mutant *let-7*(*n2853*) and analyzing its phenotypes. The *let-7*(*n2853*) is a temperature-sensitive allele and the mutant animals show both vulva and alae development defects in a stage-dependent manner in L4 and adult stages. At the non-permissive temperature (25°C) *let-7*(*n2853*) mutants die of vulva bursting. To examine the potential enhancement by *fust-1*(*tm4439*), we analyzed the vulva bursting phenotype at 25°C at the L4 stage, when the phenotype was mild, and found that *fust-1*(*tm4439*) significantly enhanced the vulva phenotype of *let-7*(*n2853*) (Figure 5D). Similarly, the alae development defect in *let-7*(*n2853*) was significantly enhanced by *fust-1*(*tm4439*), as quantified by counting animals with incomplete alae formation 16 hr after L4 at 15°C (Figure 5E). Additionally, we examined if *fust-1* affects the function of *lsy-6*, an miRNA that specifies the neuronal fate of one of two bilaterally symmetric ASE chemosensory neurons (Johnston and Hobert, 2003). In the loss-of-function hypomorphic allele *lsy-6*(*ot150*), a subset of animals exhibit the ASEL misspecification phenotype as indicated by the "off" status of the ASEL-specific *Plim-6::GFP* marker, while the remaining animals have the WT phenotype with the *Plim-6::GFP* marker being "on." We found that *fust-1*(*tm4439*) significantly enhanced the ASEL misspecification phenotype of *lsy-6*(*ot150*), as quantified by scoring the *Plim-6::GFP* status of mutants (Figure 5F). Together, these data demonstrate that *fust-1* is required for optimal miRNA-mediated gene silencing in *C. elegans*.

FUS Binds to MiR-200c

Next, we sought to uncover the mechanisms through which FUS regulates miRNA-mediated gene silencing. Since miR-200c and *ZEB1* are a conserved miRNA-mRNA pair whose levels are regulated by FUS, we asked whether FUS regulates the activity of mature miR-200c independent of its biogenesis. First, we tested whether FUS directly interacts with mature miR-200c, which is predicted to form a stem-loop structure that contains multiple AU residues (Figure S4A) and share characteristics of RNAs previously illustrated to elicit FUS binding (Hoell et al., 2011). In RNA gel-shift assays, we showed that FUS had a similar binding affinity for miR-200c as the "GGUG"-containing oligoribonucleotide (Figure 6A), which is a previously established target of FUS (Lerga et al., 2001). By comparison, FUS had a lower binding affinity for miR-505 than with miR-200c (Figure 6A). To verify the specificity of the interactions, we conducted competition assays in which we pre-incubated FUS with varying amounts of unlabeled miR-200c followed by incubation with the labeled probes. Results confirmed the specificity of the gel shifts as increasing the levels of unlabeled miR-200c decreased the association between the labeled riboprobes and FUS (Figure 6B). Moreover, as less unlabeled miR-200c was required to compete off miR-505's association with GST-FUS than with GGUG or miR-200c, our data again suggest that FUS binds to GGUG and miR-200c more tightly than to miR-505. Together, the gel-shift assays indicate that FUS can bind miR-200c directly with a relatively higher affinity than miR-505. To further confirm the differential binding of FUS to the miRNAs, we performed a single-molecule binding assay by purifying and immobilizing His-tagged FUS protein on a solid surface and measuring its binding to cy5-lableled miR-200c or miR-505 oligoribonucleotides. The single-molecule fluorescent measurements indicated that miR-200c is bound to FUS more efficiently than miR-505 (Figure 6C). We next examined whether R495X binds miR-200c less tightly than WT FUS. We compared the gel-shift binding curves between GST-FUS and GST-R495X when incubated with the miR-200c oligoribonucleotide. The R495X mutant consistently showed reduced association with miR-200c when compared with WT FUS (Figures S4B–S4D).

To validate the interaction between FUS and miR-200c *in vivo*, we performed RNA immunoprecipitation (RIP) experiments using HEK293 cells expressing WT FUS or R495X, or the SOD1 control, along with miR-200c (Figure 7A). FUS proteins were pulled down with anti-myc-agarose beads, and the immunoprecipitated miR-200c was quantified by qPCR. The results indicate that FUS bound significantly more miR-200c than the SOD1 control. Notably, R495X bound significantly less miR-200c than WT FUS. To confirm the endogenous interaction of FUS to miR-200c, we conducted RIP experiments in HAP1 WT and FUS KO cells. Compared with FUS KO cells, the FUS antibody pulled down significantly more endogenous miR-200c in the WT cells (Figure 7B). The difference in the levels of immunoprecipitated miR-200c did not reflect the difference in endogenous miR-200c levels because FUS KO cells exhibited slightly higher levels of endogenous miR-200c than WT cells (Figure S6A). Collectively, the RIP assays reveal that FUS binds miR-200c and that this association with miR-200c is reduced by the FUS mutation R495X.
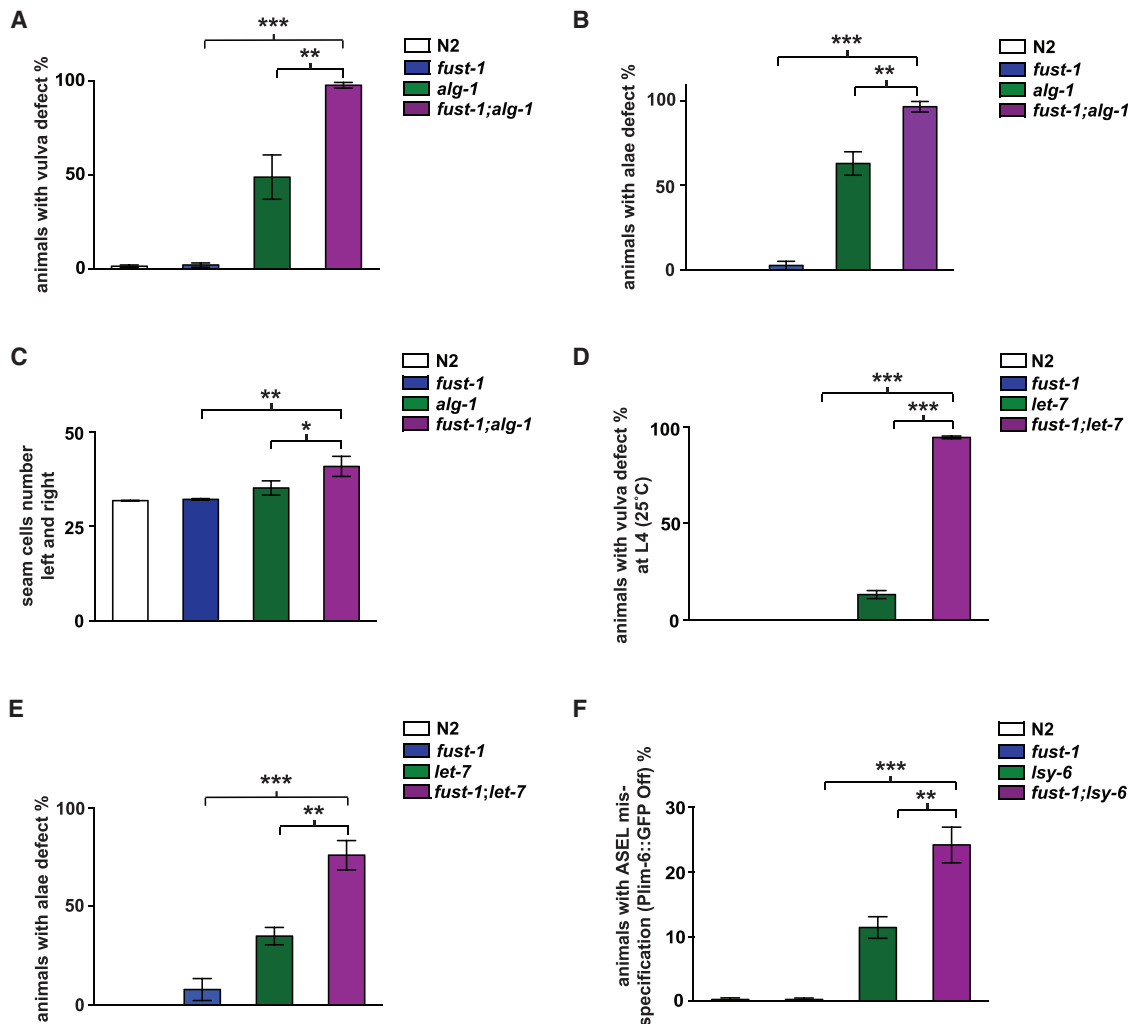
**Figure 5. *C. elegans* FUS Homolog Promotes miRNA Function**

(A) The loss-of-function *fust-1*(*tm4439*) allele enhanced the vulva development defect in *alg-1*(*gk214*), as scored by vulva bursting and worm bags in adults 3 days after L4 at 20°C (n ≥ 3).

(B) The *fust-1*(*tm4439*) allele enhanced the alae development defect in *alg-1*(*gk214*), as quantified by counting animals with incomplete alae formation 16 hr after L4 at 20°C (n ≥ 4).

(C) The *fust-1*(*tm4439*) allele enhanced the seam cell division phenotype in *alg-1*(*gk214*), as marked by the *wIs54(Pscm::GFP)* reporter. There are 16 seam cells arranged as a longitudinal row on the left or right side of the body of adult hermaphrodites, and the number of seam cells on both sides was quantified at the L4 stage at 20°C (n ≥ 15).

(D) The *fust-1*(*tm4439*) allele enhanced the vulva development defect in the hypomorphic miRNA mutant *let-7(n2853)* at the L4 stage at 25°C (n = 4).

(E) The *fust-1*(*tm4439*) allele enhanced the alae development defect in the miRNA mutant *let-7(n2853)*, as quantified by counting animals with incomplete alae formation 16 hr after L4 at 15°C (n = 5).

(F) The *fust-1*(*tm4439*) allele enhanced the ASEL specification defect in the hypomorphic miRNA mutant *lsy-6(ot150)*, as quantified by counting animals exhibiting the *Plim-6::GFP* "off" phenotype (n ≥ 4). Error bars represent ± SEM. *$p \leq 0.05$, **$p \leq 0.01$, ***$p \leq 0.001$.

See also Figure S3.

FUS Promotes Mature MiR-200c-Mediated Silencing of *ZEB1*

Next, we focused on miR-200c and its mRNA targets to study the role of FUS in mature miRNA-mediated gene silencing. First, to test whether FUS's association with its mRNA targets is affected by R495X, we analyzed two of the significantly upregulated transcripts (Figure 7C), *ZEB1* and *FZD6*, which are also targets of miR-200c. Using RIP assays in HEK293 cells expressing WT FUS or R495X, and a DNA vector control, in the presence of exogenous hsa-miR-200c, we found that WT FUS pulled down a large amount of *ZEB1* or *FZD6* mRNAs, but R495X's association with these mRNAs was greatly reduced (Figure 7C). Moreover, the association between FUS and *ZEB1* mRNA in the RIP assay was dependent on miR-200c, since treatment with a specific miR-200c antagomir, which significantly reduced the quantity of miR-200c (Figure S5F), but not a control
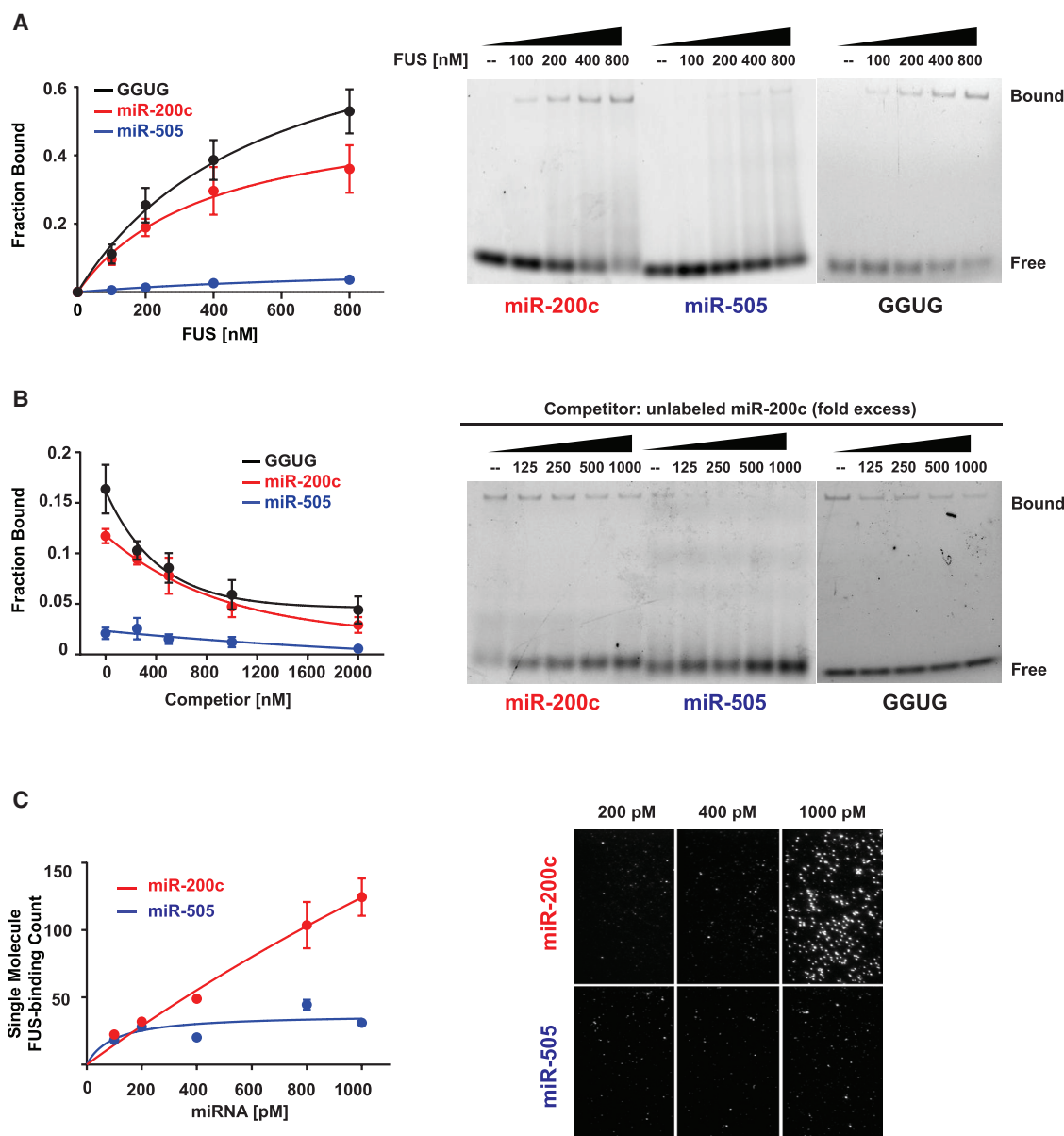
Figure 6. FUS Binds to miR-200c Directly

(A) Left: binding curves of GST-FUS (0, 100, 200, 400, and 800 nM) with fluorescently labeled oligoribonucleotides GGUG, miR-200c, and miR-505 (2 nM) (n = 3). Amount of binding is represented as fraction bound, which is measured by dividing the shifted signal by the total signal per lane. Right: representative gel-shift images with each labeled probe are shown.

(B) Left: binding curves from the competition assays in (A) (n = 3). The amount of unlabeled miR-200c is represented as fold excess relative to the labeled probe amount. Right: representative gel-shift images for competition assays of GST-FUS (200 nM) with 2 nM cy3-labeled GGUG, cy5-labeled miR-200c, or miR-505, in the presence of unlabeled miR-200c.

(C) Left: a plot of the single-molecule binding curves between immobilized His-FUS and cy5-labeled miR-200c or miR-505 at different concentrations. Each data point represents the average of ≥10 images from two independent experiments. Right: representative fluorescence images of cy5-labeled miR-200c or miR-505 bound to His-FUS. Error bars represent ± SEM.

See also Figure S4.

oligonucleotide, abolished the enrichment of *ZEB1* mRNA in FUS immunoprecipitates (Figure 7D).

We then used *ZEB1* as a model mRNA transcript to address whether its silencing by mature miR-200c is affected by FUS's association with *ZEB1*. Specifically, we asked whether blocking

FUS's interaction with *ZEB1* could impair the silencing of this transcript by miR-200c. To accomplish this, we first identified an FUS crosslinked binding site in the 3′ UTR of *ZEB1* from the FUS CLIP data (Hoell et al., 2011) and also identified an miR-200c seed site (AAUACUG) upstream of and nearby
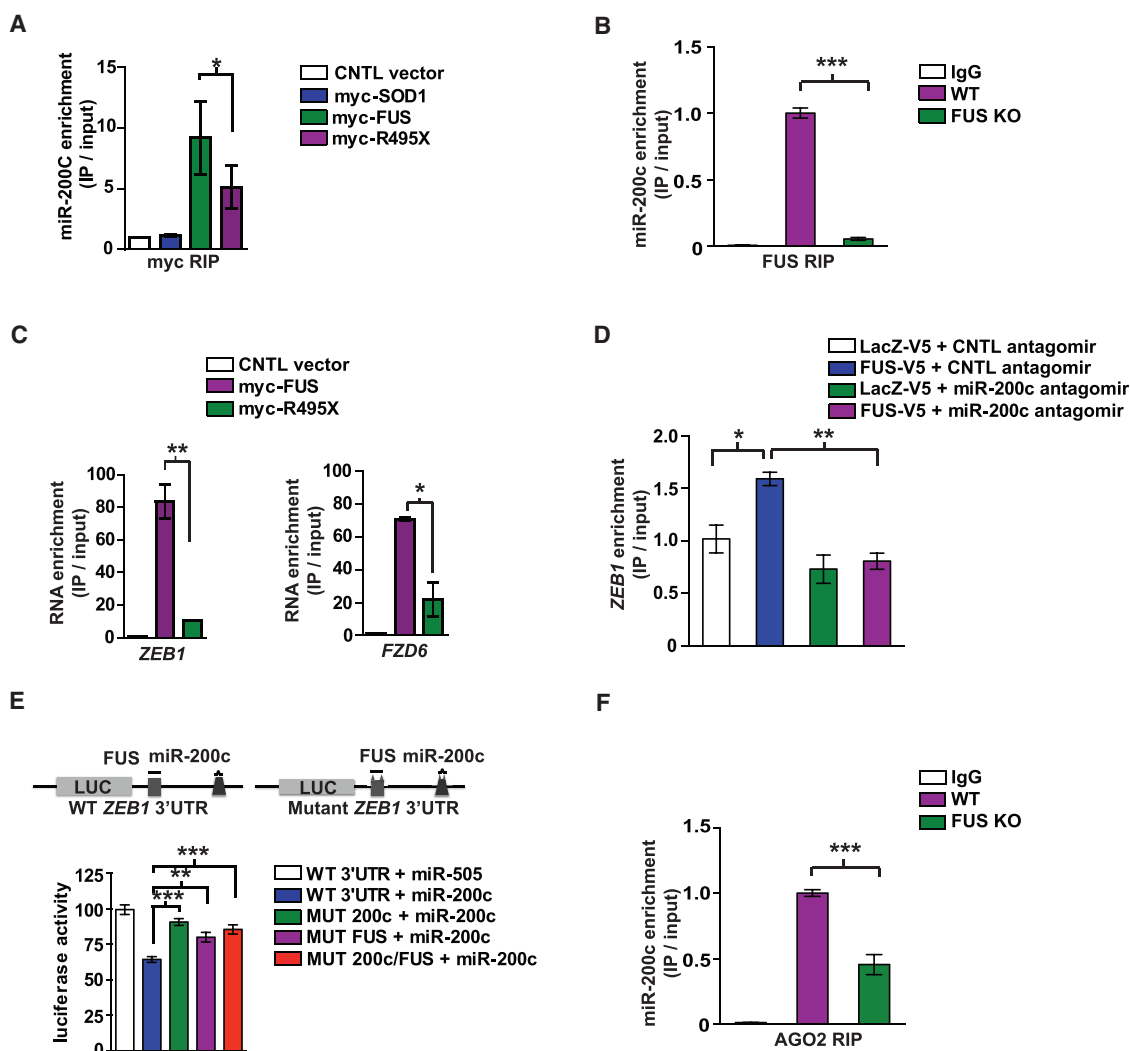
Figure 7. FUS Promotes miR-200c-Mediated Degradation of *ZEB1*

(A) Bar graphs show the amount of immunoprecipitated miR-200c (n = 5). HEK293 cells are transfected with myc-FUS, myc-R495X, myc-SOD1, or control pcDNA3.1, along with pCMV-miR-200c, prior to the IP by anti-myc antibodies.

(B) Bar graph represents enrichment of mature miR-200c in RIP experiments using an FUS antibody in human WT HAP1 cells versus FUS KO HAP1 cells (n = 3), indicating the endogenous interaction between FUS and miR-200c.

(C) Bar graphs show the amount of immunoprecipitated mRNA of *ZEB1* (left) and *FZD6* (right). HEK293 cells are transfected with pcDNA3.1, myc-FUS, or myc-R495X, along with pCMV-miR-200c, prior to IP with anti-myc antibodies.

(D) Bar graphs show the amount of immunoprecipitated mRNA of *ZEB1* in HEK293 cells transfected with FUS-V5 or LacZ-V5 together with a specific miR-200c antagomir or a control antagomir, prior to IP with anti-V5 antibodies.

(E) Top: a model of the experimental design to test the role of FUS or miR-200c binding to *ZEB1* 3′ UTR in its silencing. Bar graphs compare the normalized luciferase activity of the pmirGLO reporters with WT or mutated *ZEB1* 3′ UTRs in the presence of recombinant pCMV-miR-505 or pCMV-miR-200c, plotted as a percentage relative to the control (n = 3). Normalization was performed by dividing the firefly activity by the *Renilla* activity in each condition.

(F) Bar graph represents enrichment of miR-200c in RIP experiments using an AGO2 antibody in human FUS WT and KO HAP1 cells (n = 3). Error bars represent ± SEM. *$p \leq 0.05$, **$p \leq 0.01$, ***$p \leq 0.001$.

See also Figures S5 and S6.

this crosslinked cluster. We cloned a 128 nt region containing both the FUS-crosslinked site and the seed site downstream of the firefly luciferase gene in the pmiRGLO luciferase reporter (Figure S5A). As this reporter houses both a firefly and *Renilla* luciferase gene under separate promoters, we were able to evaluate quantitatively the effectiveness of miR-200c-mediated

silencing through this 128 nt target region based on a reduction in the firefly luciferase activity, with normalization to the *Renilla* activity. In addition to generating the *ZEB1* WT 3′ UTR reporter, we also made point mutations in the miR-200c seed site (*ZEB1* MUT 200c 3′ UTR) or substituted the residues that were crosslinked by FUS (*ZEB1* MUT FUS 3′ UTR), to ask whether changes

in either region would reduce the ability of miR-200c to silence this portion of the *ZEB1* 3′ UTR.

Luciferase assays indicated that co-expression of the WT *ZEB1* 3′ UTR reporter with a plasmid that expresses miR-200c in HEK293 cells reduced the firefly activity relative to the activity caused by co-transfection with miR-505 as a control (Figure 7E). As a negative control, the same reporter vector lacking the *ZEB1* 3′ UTR sequence showed no difference in the luciferase activity when co-transfected with miR-200c versus miR-505. Notably, point mutations in the miR-200c seed site (*ZEB1* MUT 200c) significantly reduced the silencing of the *ZEB1* 3′ UTR reporter by miR-200c (Figure 7E). Importantly, mutations in specific FUS-binding residues (*ZEB1* MUT FUS) also significantly reduced the silencing of the *ZEB1* 3′ UTR reporter by miR-200c (Figure 7E). Furthermore, double mutations in both miR-200c seed site and FUS-binding residues similarly reduced the silencing of the *ZEB1* 3′ UTR reporter (Figure 7E). Moreover, the knockdown of FUS abolished the changes of *ZEB1* 3′ UTR WT or mutated reporters (Figure S5B), indicating that FUS is required for the silencing of the *ZEB1* 3′ UTR reporter by miR-200c. In addition to the luciferase activity, the *ZEB1* 3′ UTR reporter mRNA levels were upregulated when the miR-200c seed site or FUS-binding residues were mutated (Figure S5C), consistent with the notion that miRNA-induced translational repression is associated with target mRNA degradation. Similar to the miR-200c-*ZEB1* pair, the dependence on FUS binding to the transcript for its miRNA-induced silencing was confirmed on another miRNA-mRNA pair, miR-20b and *TXNIP*, using a similar luciferase reporter system containing the *TXNIP* 3′ UTR (Figure S5D). In summary, these results demonstrate that impairment of FUS's interaction with target mRNA is sufficient to reduce the silencing activity of mature miRNAs independent of miRNA biogenesis.

To explore the mechanisms of how FUS regulates the miRNA activity, we asked whether FUS facilitates the binding of miR-200c to AGO2. We conducted RIP experiments in HAP1 WT and FUS KO cells. Endogenous AGO2 proteins were pulled down using anti-AGO2 antibodies, without any difference detected in the levels of AGO2 in inputs or immunoprecipitates between FUS WT and KO cells, and then the level of endogenous miR-200c present in the immunoprecipitates was quantified by qPCR. Compared with WT cells, AGO2 pulled down much less miR-200c in the FUS KO cells (Figure 7F). Since the input level of endogenous miR-200c was not decreased but slightly increased in the FUS KO cells (Figure S6A), the AGO2 RIP experiment demonstrates that AGO2's association with miR-200c is in part FUS dependent. Interestingly, despite the increase of miR-200c in FUS KO cells, the level of its target *ZEB1* mRNA was not decreased but slightly increased (Figure S6B), consistent with the findings suggesting that FUS is required for optimal mature miRNA-mediated silencing. Consistent with the AGO2 RIP result, when miR-200c was pulled down from cell lysates using a biotinylated 2′-O-methylated oligonucleotide complementary to miR-200c, as validated by depletion of miR-200c from the lysates (Figure S5G), more AGO2 or FUS proteins were co-precipitated when miR-200c was overexpressed; however, this increase in the level of AGO2 associated with miR-200c was decreased in the FUS KO cells (Figure S5E), suggesting that

FUS is required for the optimal association between miR-200c and AGO2.

DISCUSSION

Our present study reveals a role for FUS in the miRNA silencing pathway in which it binds to Argonaute and regulates mature miRNA-mediated gene silencing activity. We propose that FUS facilitates the association among miRISC components such as AGO2, a subset of mature miRNAs, and their mRNA targets, thereby promoting efficiency in miRNA-mediated silencing (Figure S7). Since FUS interacts with AGO2, it may have a global impact on miRNA activities. At the same time, FUS could confer selective silencing through interaction with specific miRNAs or mRNAs. Considering the challenge for miRISC to locate targets among the RNAs in the cell, there is likely a group of RBPs that act like FUS and specialize in miRNA targeting and silencing for their respective gene targets.

FUS is a multi-functional protein involved in a range of activities from DNA repair to RNA splicing. Our present study indicates a direct role of FUS in regulating miRNA activities in gene silencing. The implication of FUS in the miRNA silencing pathway underscores the notion that it acts at multiple levels of RNA processing to regulate gene expression. We found that FUS is required for optimal miRNA silencing and this function is mediated by the interaction of FUS with the core miRISC component AGO2 as well as the miRNA and mRNA components. Notably, FUS's association with AGO2 occurs via the latter's MID domain, a site that also binds FMRP, an RBP implicated in fragile X syndrome (Li et al., 2014). By recruiting different RBPs through its MID domain, AGO2 could potentially enhance miRNA silencing of specific targets. Furthermore, FUS appears to have a conserved function in regulating miRNA silencing in *C. elegans*, since genetic analyses suggest that the *C. elegans* homolog, *fust-1*, promotes miRNA-mediated gene silencing. Therefore, the functions of RBPs as represented by FUS may be an ancient and evolutionarily conserved mechanism for regulating miRNA-mediated gene expression.

Dysregulation of RNA metabolism including miRNA processing has been increasingly associated with the neurodegenerative diseases, such as ALS, which is associated with mutations and proteinopathy of RBPs including TDP-43 and FUS. TDP-43 was reported to promote miRNA biogenesis as a component of Drosha and Dicer complexes (Kawahara and Mieda-Sato, 2012) and bind mature miRNAs (King et al., 2014). FUS was reported to interact with Drosha at the transcription sites of pri-miRNAs (Morlando et al., 2012) and interfere with Dicer activity (Emde et al., 2015). Our present study establishes a previously unrecognized role of FUS in regulating the activity of mature miRNAs downstream of the miRNA biogenesis. Both gain of toxicity and loss of normal FUS function as a consequence of the mutations have been proposed to underlie neurodegeneration in animal models (Armstrong and Drapeau, 2013; Huang et al., 2011; Lanson et al., 2011; Sharma et al., 2016). Our study shows that R495X, the mutation linked to severe ALS, impairs the function of FUS in miRNA silencing (Figure 3). In addition, the R495X mutation impairs the association of FUS with AGO2, miR-200c, and RNA targets such as *ZEB1*. Together, our results

highlight the role of FUS in regulating miRNA independently of miRNA biogenesis.

In summary, our studies establish FUS as a direct player in miRNA silencing, in which it associates with miRISC protein components as well as miRNAs and their mRNA targets, promoting efficient miRNA-mediated gene silencing. Our findings illustrate a layer of regulation of miRNA-mediated silencing through the RBP FUS and implicate the mechanism of miRNA regulation in the pathogenesis of diseases such as neurodegeneration.

STAR★METHODS

Detailed methods are provided in the online version of this paper and include the following:

- KEY RESOURCES TABLE
- CONTACT FOR REAGENT AND RESOURCE SHARING
- EXPERIMENTAL MODEL AND SUBJECT DETAILS
  - Mice and cell lines
  - C. elegans
- METHOD DETAILS
  - Mouse ES cell culture, motor neuron differentiation, and lentiviral transduction
  - Plasmid and antibody
  - Microarray and qPCR analysis
  - Luciferase assay
  - Protein and RNA co-immunoprecipitation and immunocytochemistry
  - Electrophoretic mobility shift assay
  - Single molecule binding assay
  - C. elegans
  - Bioinformatic analysis
- QUANTIFICATION AND STATISTICAL ANALYSIS
  - Statistical analysis
- DATA AND SOFTWARE AVAILABILITY
  - Data Resources

SUPPLEMENTAL INFORMATION

Supplemental Information includes seven figures and five tables and can be found with this article online at https://doi.org/10.1016/j.molcel.2018.02.001.

AUTHOR CONTRIBUTIONS

T.Z., Y.-C.W., A.K.L.L., and J.W. designed the study. T.Z., Y.-C.W., P.M., Y.J.J., H.L., L.H., A.A., and G.P. performed experiments. A.K.L.L. and S.-E.O. conducted the proteomic analysis. H.-Y.H. performed bioinformatics analysis. J.K.K. contributed to the design of miRNA assays in *C. elegans* and A.F.A. performed the *lsy-6* reporter assay. S.M. designed and A.G.N. performed the single molecular binding assay. L.G., H.W., J.S., E.E., and L.J. provided purified proteins. All authors helped with analyzing the results and preparing the manuscript. T.Z., Y.-C.W., and J.W. wrote the paper with contributions from A.K.L. and P.M.

DECLARATION OF INTERESTS

The authors declare no competing interests.

REFERENCES

Armstrong, G.A., and Drapeau, P. (2013). Loss and gain of FUS function impair neuromuscular synaptic transmission in a genetic model of ALS. Hum. Mol. Genet. *22*, 4282–4292.

Bartel, D.P. (2009). MicroRNAs: target recognition and regulatory functions. Cell *136*, 215–233.

Bhattacharyya, S.N., Habermacher, R., Martine, U., Closs, E.I., and Filipowicz, W. (2006). Relief of microRNA-mediated translational repression in human cells subjected to stress. Cell *125*, 1111–1124.

Blin, K., Dieterich, C., Wurmus, R., Rajewsky, N., Landthaler, M., and Akalin, A. (2015). DoRiNA 2.0—upgrading the doRiNA database of RNA interactions in post-transcriptional regulation. Nucleic Acids Res. *43*, D160–D167.

Bosco, D.A., Lemay, N., Ko, H.K., Zhou, H., Burke, C., Kwiatkowski, T.J., Jr., Sapp, P., McKenna-Yasek, D., Brown, R.H., Jr., and Hayward, L.J. (2010). Mutant FUS proteins that cause amyotrophic lateral sclerosis incorporate into stress granules. Hum. Mol. Genet. *19*, 4160–4175.

Deng, H.-X., Zhai, H., Bigio, E.H., Yan, J., Fecto, F., Ajroud, K., Mishra, M., Ajroud-Driss, S., Heller, S., Sufit, R., et al. (2010). FUS-immunoreactive inclusions are a common feature in sporadic and non-SOD1 familial amyotrophic lateral sclerosis. Ann. Neurol. *67*, 739–748.

Dichmann, D.S., and Harland, R.M. (2012). fus/TLS orchestrates splicing of developmental regulators during gastrulation. Genes Dev. *26*, 1351–1363.

Dormann, D., Rodde, R., Edbauer, D., Bentmann, E., Fischer, I., Hruscha, A., Than, M.E., Mackenzie, I.R.A., Capell, A., Schmid, B., et al. (2010). ALS-associated fused in sarcoma (FUS) mutations disrupt Transportin-mediated nuclear import. EMBO J. *29*, 2841–2857.

Elkayam, E., Kuhn, C.D., Tocilj, A., Haase, A.D., Greene, E.M., Hannon, G.J., and Joshua-Tor, L. (2012). The structure of human argonaute-2 in complex with miR-20a. Cell *150*, 100–110.

Emde, A., Eitan, C., Liou, L.L., Libby, R.T., Rivkin, N., Magen, I., Reichenstein, I., Oppenheim, H., Eilam, R., Silvestroni, A., et al. (2015). Dysregulated miRNA biogenesis downstream of cellular stress and ALS-causing mutations: a new mechanism for ALS. EMBO J. *34*, 2633–2651.

Gal, J., Zhang, J., Kwinter, D.M., Zhai, J., Jia, H., Jia, J., and Zhu, H. (2011). Nuclear localization sequence of FUS and induction of stress granules by ALS mutants. Neurobiol. Aging *32*, 2323.e27–2323.e40.

Grishok, A., Pasquinelli, A.E., Conte, D., Li, N., Parrish, S., Ha, I., Baillie, D.L., Fire, A., Ruvkun, G., and Mello, C.C. (2001). Genes and mechanisms related to RNA interference regulate expression of the small temporal RNAs that control *C. elegans* developmental timing. Cell *106*, 23–34.

Hafner, M., Landthaler, M., Burger, L., Khorshid, M., Hausser, J., Berninger, P., Rothballer, A., Ascano, M., Jr., Jungkamp, A.C., Munschauer, M., et al. (2010). Transcriptome-wide identification of RNA-binding protein and microRNA target sites by PAR-CLIP. Cell *141*, 129–141.

Herzog, V.A., and Ameres, S.L. (2015). Approaching the golden fleece a molecule at a time: biophysical insights into Argonaute-instructed nucleic acid interactions. Mol. Cell 59, 4–7.

Hoell, J.I., Larsson, E., Runge, S., Nusbaum, J.D., Duggimpudi, S., Farazi, T.A., Hafner, M., Borkhardt, A., Sander, C., and Tuschl, T. (2011). RNA targets of wild-type and mutant FET family proteins. Nat. Struct. Mol. Biol. 18, 1428–1431.

Huang, C., Zhou, H., Tong, J., Chen, H., Liu, Y.-J., Wang, D., Wei, X., and Xia, X.-G. (2011). FUS transgenic rats develop the phenotypes of amyotrophic lateral sclerosis and frontotemporal lobar degeneration. PLoS Genet. 7, e1002011.

Iko, Y., Kodama, T.S., Kasai, N., Oyama, T., Morita, E.H., Muto, T., Okumura, M., Fujii, R., Takumi, T., Tate, S., and Morikawa, K. (2004). Domain architectures and characterization of an RNA-binding protein, TLS. J. Biol. Chem. 279, 44834–44840.

Ito, D., Seki, M., Tsunoda, Y., Uchiyama, H., and Suzuki, N. (2011). Nuclear transport impairment of amyotrophic lateral sclerosis-linked mutations in FUS/TLS. Ann. Neurol. 69, 152–162.

Janas, M.M., Wang, B., Harris, A.S., Aguiar, M., Shaffer, J.M., Subrahmanyam, Y.V., Behlke, M.A., Wucherpfennig, K.W., Gygi, S.P., Gagnon, E., and Novina, C.D. (2012). Alternative RISC assembly: binding and repression of microRNA-mRNA duplexes by human Ago proteins. RNA 18, 2041–2055.

Johnston, R.J., and Hobert, O. (2003). A microRNA controlling left/right neuronal asymmetry in Caenorhabditis elegans. Nature 426, 845–849.

Kawahara, Y., and Mieda-Sato, A. (2012). TDP-43 promotes microRNA biogenesis as a component of the Drosha and Dicer complexes. Proc. Natl. Acad. Sci. USA 109, 3347–3352.

Kedde, M., Strasser, M.J., Boldajipour, B., Oude Vrielink, J.A., Slanchev, K., le Sage, C., Nagel, R., Voorhoeve, P.M., van Duijse, J., Ørom, U.A., et al. (2007). RNA-binding protein Dnd1 inhibits microRNA access to target mRNA. Cell 131, 1273–1286.

King, I.N., Yartseva, V., Salas, D., Kumar, A., Heidersbach, A., Ando, D.M., Stallings, N.R., Elliott, J.L., Srivastava, D., and Ivey, K.N. (2014). The RNA-binding protein TDP-43 selectively disrupts microRNA-1/206 incorporation into the RNA-induced silencing complex. J. Biol. Chem. 289, 14263–14271.

Kishore, S., Jaskiewicz, L., Burger, L., Hausser, J., Khorshid, M., and Zavolan, M. (2011). A quantitative analysis of CLIP methods for identifying binding sites of RNA-binding proteins. Nat. Methods 8, 559–564.

Kwiatkowski, T.J., Jr., Bosco, D.A., Leclerc, A.L., Tamrazian, E., Vanderburg, C.R., Russ, C., Davis, A., Gilchrist, J., Kasarskis, E.J., Munsat, T., et al. (2009). Mutations in the FUS/TLS gene on chromosome 16 cause familial amyotrophic lateral sclerosis. Science 323, 1205–1208.

Lagier-Tourenne, C., Polymenidou, M., Hutt, K.R., Vu, A.Q., Baughn, M., Huelga, S.C., Clutario, K.M., Ling, S.C., Liang, T.Y., Mazur, C., et al. (2012). Divergent roles of ALS-linked proteins FUS/TLS and TDP-43 intersect in processing long pre-mRNAs. Nat. Neurosci. 15, 1488–1497.

Lanson, N.A., Jr., Maltare, A., King, H., Smith, R., Kim, J.H., Taylor, J.P., Lloyd, T.E., and Pandey, U.B. (2011). A Drosophila model of FUS-related neurodegeneration reveals genetic interaction between FUS and TDP-43. Hum. Mol. Genet. 20, 2510–2523.

Lerga, A., Hallier, M., Delva, L., Orvain, C., Gallais, I., Marie, J., and Moreau-Gachelin, F. (2001). Identification of an RNA binding specificity for the potential splicing factor TLS. J. Biol. Chem. 276, 6807–6816.

Leung, A.K.L. (2015). The whereabouts of microRNA actions: cytoplasm and beyond. Trends Cell Biol. 25, 601–610.

Leung, A.K., Vyas, S., Rood, J.E., Bhutkar, A., Sharp, P.A., and Chang, P. (2011). Poly(ADP-ribose) regulates stress responses and microRNA activity in the cytoplasm. Mol. Cell 42, 489–499.

Li, Y., Tang, W., Zhang, L.R., and Zhang, C.Y. (2014). FMRP regulates miR196a-mediated repression of HOXB8 via interaction with the AGO2 MID domain. Mol. Biosyst. 10, 1757–1764.

Mackenzie, I.R., Rademakers, R., and Neumann, M. (2010). TDP-43 and FUS in amyotrophic lateral sclerosis and frontotemporal dementia. Lancet Neurol. 9, 995–1007.

Mastrocola, A.S., Kim, S.H., Trinh, A.T., Rodenkirch, L.A., and Tibbetts, R.S. (2013). The RNA-binding protein fused in sarcoma (FUS) functions downstream of poly(ADP-ribose) polymerase (PARP) in response to DNA damage. J. Biol. Chem. 288, 24731–24741.

Masuda, A., Takeda, J., Okuno, T., Okamoto, T., Ohkawara, B., Ito, M., Ishigaki, S., Sobue, G., and Ohno, K. (2015). Position-specific binding of FUS to nascent RNA regulates mRNA length. Genes Dev. 29, 1045–1057.

McCreedy, D.A., Brown, C.R., Butts, J.C., Xu, H., Huettner, J.E., and Sakiyama-Elbert, S.E. (2014). A new method for generating high purity motoneurons from mouse embryonic stem cells. Biotechnol. Bioeng. 111, 2041–2055.

Morlando, M., Dini Modigliani, S., Torrelli, G., Rosa, A., Di Carlo, V., Caffarelli, E., and Bozzoni, I. (2012). FUS stimulates microRNA biogenesis by facilitating co-transcriptional Drosha recruitment. EMBO J. 31, 4502–4510.

Moser, J.J., Chan, E.K., and Fritzler, M.J. (2009). Optimization of immunoprecipitation-western blot analysis in detecting GW182-associated components of GW/P bodies. Nat. Protoc. 4, 674–685.

Panwar, B., Omenn, G.S., and Guan, Y. (2017). miRmine: a database of human miRNA expression profiles. Bioinformatics 33, 1554–1560.

Prasad, D.D., Ouchida, M., Lee, L., Rao, V.N., and Reddy, E.S. (1994). TLS/FUS fusion domain of TLS/FUS-erg chimeric protein resulting from the t(16;21) chromosomal translocation in human myeloid leukemia functions as a transcriptional activation domain. Oncogene 9, 3717–3729.

Qiu, H., Lee, S., Shang, Y., Wang, W.Y., Au, K.F., Kamiya, S., Barmada, S.J., Finkbeiner, S., Lui, H., Carlton, C.E., et al. (2014). ALS-associated mutation FUS-R521C causes DNA damage and RNA splicing defects. J. Clin. Invest. 124, 981–999.

Reinhart, B.J., Slack, F.J., Basson, M., Pasquinelli, A.E., Bettinger, J.C., Rougvie, A.E., Horvitz, H.R., and Ruvkun, G. (2000). The 21-nucleotide let-7 RNA regulates developmental timing in Caenorhabditis elegans. Nature 403, 901–906.

Schwartz, J.C., Ebmeier, C.C., Podell, E.R., Heimiller, J., Taatjes, D.J., and Cech, T.R. (2012). FUS binds the CTD of RNA polymerase II and regulates its phosphorylation at Ser2. Genes Dev. 26, 2690–2695.

Sharma, A., Lyashchenko, A.K., Lu, L., Nasrabady, S.E., Elmaleh, M., Mendelsohn, M., Nemes, A., Tapia, J.C., Mentis, G.Z., and Shneider, N.A. (2016). ALS-associated mutant FUS induces selective motor neuron degeneration through toxic gain of function. Nat. Commun. 7, 10465.

Stalder, L., Heusermann, W., Sokol, L., Trojer, D., Wirz, J., Hean, J., Fritzsche, A., Aeschimann, F., Pfanzagl, V., Basselet, P., et al. (2013). The rough endoplasmic reticulum is a central nucleation site of siRNA-mediated RNA silencing. EMBO J. 32, 1115–1127.

Sun, Z., Diaz, Z., Fang, X., Hart, M.P., Chesi, A., Shorter, J., and Gitler, A.D. (2011). Molecular determinants and genetic modifiers of aggregation and toxicity for the ALS disease protein FUS/TLS. PLoS Biol. 9, e1000614.

Sun, S., Ling, S.C., Qiu, J., Albuquerque, C.P., Zhou, Y., Tokunaga, S., Li, H., Qiu, H., Bui, A., Yeo, G.W., et al. (2015). ALS-causative mutations in FUS/TLS confer gain and loss of function by altered association with SMN and U1-snRNP. Nat. Commun. 6, 6171.

Tan, A.Y., and Manley, J.L. (2010). TLS inhibits RNA polymerase III transcription. Mol. Cell. Biol. 30, 186–196.

Uranishi, H., Tetsuka, T., Yamashita, M., Asamitsu, K., Shimizu, M., Itoh, M., and Okamoto, T. (2001). Involvement of the pro-oncoprotein TLS (translocated in liposarcoma) in nuclear factor-kappa B p65-mediated transcription as a coactivator. J. Biol. Chem. 276, 13395–13401.

Vance, C., Rogelj, B., Hortobágyi, T., De Vos, K.J., Nishimura, A.L., Sreedharan, J., Hu, X., Smith, B., Ruddy, D., Wright, P., et al. (2009). Mutations in FUS, an RNA processing protein, cause familial amyotrophic lateral sclerosis type 6. Science 323, 1208–1211.

Vasudevan, S., Tong, Y., and Steitz, J.A. (2007). Switching from repression to activation: microRNAs can up-regulate translation. Science *318*, 1931–1934.

Waibel, S., Neumann, M., Rosenbohm, A., Birve, A., Volk, A.E., Weishaupt, J.H., Meyer, T., Müller, U., Andersen, P.M., and Ludolph, A.C. (2013). Truncating mutations in FUS/TLS give rise to a more aggressive ALS-phenotype than missense mutations: a clinico-genetic study in Germany. Eur. J. Neurol. *20*, 540–546.

Wang, W.Y., Pan, L., Su, S.C., Quinn, E.J., Sasaki, M., Jimenez, J.C., Mackenzie, I.R., Huang, E.J., and Tsai, L.H. (2013). Interaction of FUS and HDAC1 regulates DNA damage response and repair in neurons. Nat. Neurosci. *16*, 1383–1391.

Wang, X., Schwartz, J.C., and Cech, T.R. (2015). Nucleic acid-binding specificity of human FUS protein. Nucleic Acids Res. *43*, 7535–7543.

Williams, A.H., Valdez, G., Moresi, V., Qi, X., McAnally, J., Elliott, J.L., Bassel-Duby, R., Sanes, J.R., and Olson, E.N. (2009). MicroRNA-206 delays ALS progression and promotes regeneration of neuromuscular synapses in mice. Science *326*, 1549–1554.

Yang, L., Gal, J., Chen, J., and Zhu, H. (2014). Self-assembled FUS binds active chromatin and regulates gene transcription. Proc. Natl. Acad. Sci. USA *111*, 17809–17814.

Yigit, E., Batista, P.J., Bei, Y., Pang, K.M., Chen, C.C., Tolia, N.H., Joshua-Tor, L., Mitani, S., Simard, M.J., and Mello, C.C. (2006). Analysis of the C. elegans Argonaute family reveals that distinct Argonautes act sequentially during RNAi. Cell *127*, 747–757.

Yoon, J.H., Jo, M.H., White, E.J., De, S., Hafner, M., Zucconi, B.E., Abdelmohsen, K., Martindale, J.L., Yang, X., Wood, W.H., 3rd, et al. (2015). AUF1 promotes let-7b loading on Argonaute 2. Genes Dev. *29*, 1599–1604.

Zhou, Y., Liu, S., Liu, G., Oztürk, A., and Hicks, G.G. (2013). ALS-associated FUS mutations result in compromised FUS alternative splicing and autoregulation. PLoS Genet. *9*, e1003895.

STAR★METHODS

KEY RESOURCES TABLE

REAGENT or RESOURCE	SOURCE	IDENTIFIER
Antibodies		
Negative control for mouse IgG	Neomarkers, CA	RRID: AB_141706
Negative control for rabbit IgG	Neomarkers, CA	RRID: AB_60825
FUS (rabbit polyclonal)	Bethyl Laboratories	RRID: AB_263409
FUS (rabbit polyclonal)	Bethyl Laboratories	RRID: AB_263410
FUS/TLS (4H11) mouse monoclonal	Santa Cruz	RRID: AB_2105208
Ago2 (mouse monoclonal)	WAKO chemicals	RRID: AB_1106836
Ago2 (rabbit polyclonal)	Cell Signaling	RRID: AB_2096291
Ago2 (rat monoclonal)	SIGMA-Aldrich	RRID: AB_10600719
Ago1 (rat monoclonal)	SIGMA-Aldrich	RRID: AB_10602786
Drosha	Bethyl Laboratories	RRID: AB_1309798
c-Myc (mouse monoclonal)	SIGMA-Aldrich	RRID: AB_260581
c-Myc (mouse monoclonal)	SIGMA-Aldrich	RRID: AB_439694
Myc-HRP	Roche	RRID: AB_390910
GAPDH (rabbit polyclonal)	Thermo Fisher	RRID: AB_1090202
GFP rabbit polyclonal	LifeTech	RRID: AB_221570
GFP mouse monoclonal	Roche	RRID: AB_390913
V5-HRP	LifeTech	460708
V5 mouse monoclonal	LifeTech	460705
actin-HRP	Santa Cruz	RRID: AB_2714189
Chemicals, Peptides, and Recombinant Proteins		
GST-FUS WT	This study	N/A
GST-FUS R495X	This study	N/A
His-FUS	This study	N/A
GST	This study	N/A
AGO2	This study	N/A
Critical Commercial Assays		
RNeasy plus mini Kit	QIAGEN	74134
miRNeasy mini Kit	QIAGEN	217004
miScript II RT Kit	QIAGEN	218161
QuantiTec RT Kit	QIAGEN	205311
Dual-Luciferase Reporter Assay System	Promega	E1910
Deposited Data		
Affymetrix Exon Array and Agilent MicroRNA Microarray data	Gene Expression Omnibus repository	GEO: GSE68504
Experimental Models: Cell Lines		
WT HAP1	Horizon Discovery	N/A
FUS KO HAP1	Horizon Discovery	HZGHC001314c006
HEK293	ATCC	CRL-3216
mouse embryonic fibroblast cells	This study	N/A
FUS KO mouse embryonic fibroblast cells	This study	N/A
mouse ES cells	This study	N/A
mouse motor neurons	This study	N/A

(*Continued on next page*)

Continued

REAGENT or RESOURCE	SOURCE	IDENTIFIER
Experimental Models: Organisms/Strains		
FUS KO mouse	Generated by University of California Davis KOMP Repository	N/A
C57Bl6 mouse	Jackson Laboratory	000664
C. elegans N2 Bristol	CGC	N/A
C. elegans alg-1(gk214)	CGC	RF54
C. elegans let-7(n2853)	CGC	MT7626
C. elegans otIs114I	CGC	OH812
C. elegans otIs114I;lsy-6(ot150)	CGC	OH3646
C. elegans fust-1(tm4439)	National Bioresource Project of Japan	FX4439
C. elegans fust-1(tm4439);alg-1(gk214)	This study	IW480
C. elegans fust-1(tm4439);let-7(n2853)	This study	IW754
C. elegans otIs114[Plim-6::GFP];fust-1(tm4439)	This study	QK138/QK139
C. elegans otIs114[Plim-6::GFP];fust-1(tm4439);lsy-6(ot150)	This study	QK136/QK137
C. elegans fust-1(tm4439);wIs54[Pscm::GFP]	This study	IW755
C. elegans wIs54[Pscm::GFP];alg-1(gk214)	This study	IW756
C. elegans fust-1(tm4439);wIs54[Pscm::GFP];alg-1(gk214)	This study	IW757
Recombinant DNA		
eGFP-PARP-13	(Leung et al., 2011)	N/A
eGFP-G3BP1	(Leung et al., 2011)	N/A
eGFP-AGO2	(Leung et al., 2011)	N/A
pRCP-6X	(Leung et al., 2011)	N/A
pRCP-0X	(Leung et al., 2011)	N/A
V5-FUS	(Ito et al., 2011)	N/A
pcDNA3.1-V5-LacZ	Invitrogen	N/A
Pp-Mt-HDAC4	(Williams et al., 2009)	N/A
Pp-WT-HDAC4	(Williams et al., 2009)	N/A
pRK5-myc	This study	N/A
pRK5-myc-SOD1	This study	N/A
pRK5-myc-FUS WT	This study	N/A
pRK5-myc-FUS R495X	This study	N/A
pRK5-myc-FUS WT R521C	This study	N/A
pRFP-C-RS	Origene	TR30014
pRFP-C-RS-shFUS	This study	N/A
pmirGLO Dual-Luciferase	Promega	E1330
pmirGLO-zeb1 3′ UTR WT	This study	N/A
pmirGLO-zeb1 3′ UTR miR-200c binding mutant	This study	N/A
pmirGLO-zeb1 3′ UTR FUS binding mutant	This study	N/A
pmirGLO-zeb1 3′ UTR miR-200c/FUS binding mutant	This study	N/A
pmirGLO-txnip 3′ UTR WT	This study	N/A
pmirGLO-txnip 3′ UTR miR-20b binding mutant	This study	N/A
pmirGLO-txnip 3′ UTR FUS binding mutant	This study	N/A
pmax-GFP	Amaxa	N/A
His-FUS	Jacob Schwartz and Nicolas Fawzi	N/A
pLenti-CMV-Puro-Dest	Addgene	17452
pLenti-CMV-Puro-FUS	This study	N/A
pLenti-CMV-Puro-FUS R495X	This study	N/A
pCMV-hsa-miR-505	Origene	SC400432

Continued

REAGENT or RESOURCE	SOURCE	IDENTIFIER
pCMV-has-miR-200c	Origene	SC400258
Oligonucleotides		
CHRNA10, fwd: TTGGCTGTTACCTTTCCCTGCTG; rev: TCCTGCTCTGGAAACTCGACTGAG	N/A	N/A
FYN, fwd: ACTCTATCCAGGCAGAAGAGTGG; rev: ACAATAGCTGTCGCTCAGCATC	N/A	N/A
HOXA2, fwd: TGCCTCAGCCACAAAGAATCCC; rev: AGCTGTGTGTTGGTGTAAGCAG	N/A	N/A
CHN2, fwd: GAATCATTTGTCCTCGGGAGGTG; rev: TTGCCGCTGGCTTTCTCTAAGG	N/A	N/A
ZEB1, fwd: TTGCTCCCTGTGCAGTTACACC; rev: CCAGACTGCGTCACATGTCTTTG	N/A	N/A
TNF, fwd: CCAGGCAGTCAGATCATCTTCTCG; rev: ATCTCTCAGCTCCACGCCATTG	N/A	N/A
ARID4A, fwd: AGAGAGAGCAGAGAGAAGGGTCAG; rev: GCTGCAGCACTTGTTCGCTTTG	N/A	N/A
SYT1, fwd: TGCAAAGTGCTGAGAAGGAAGAGC; rev: TAGGTACGTAGCGAAAGGGAGAAGC	N/A	N/A
FGF18, fwd: AAGTATGCCCAGCTCCTAGTGG; rev: TGAACACACACTCCTTGCTGGTG	N/A	N/A
FZD6, fwd: TCTCTGCTGTCTTCTGGGTTGG; rev: TTCACTGATTGGATCTCTCTTGCG	N/A	N/A
GAPDH, fwd: GAAGGTGAAGGTCGGAGTC; rev: GAAGATGGTGATGGGATTTC	N/A	N/A
FLuc, fwd: GCCATGAAGCGCTACGCCCTGG; rev: TCTTGCTCACGAATACGACGGTGG	N/A	N/A
RLuc, fwd: TCAGTGGTGGGCTCGCTGCA; rev: CTTTGGAAGGTTCAGCAGCTCG	N/A	N/A
eft-2, fwd: ACGCTCGTGATGAGTTCAAG; rev: ATTTGGTCCAGTTCCGTCTG	N/A	N/A
lin-41, fwd: GGTTCCAAATGCCACAAGAG; rev: AGGTCCAACTGCCAAATCAG	N/A	N/A
Software and Algorithms		
IPA (Ingenuity Pathway Analysis)	N/A	N/A
Partek Genomics Suite v6.6	N/A	N/A

CONTACT FOR REAGENT AND RESOURCE SHARING

Further information and requests for reagents may be directed to and will be fulfilled by the Lead Contact, Jiou Wang (jiouw@jhu.edu).

EXPERIMENTAL MODEL AND SUBJECT DETAILS

Mice and cell lines

FUS KO mice, which bear an allele Fus[tm1(KOMP)Vlcg] that lacks all 15 exons of the FUS gene, were obtained from University of California Davis KOMP Repository. The KO mice were backcrossed over ten generations and maintained on the *C57Bl6* background. The animal protocol was approved by the Animal Care and Use Committee of the Johns Hopkins Medical Institutions. Mouse embryonic fibroblast (MEF) cells were isolated at embryonic day 12 following mating between heterozygous mice. To immortalize the MEF cells, the plasmid pSG5 Large T was transfected into the MEF cells, and the immortalized clones were selected by passaging.

Human FUS KO cells were created using CRISPR/Cas9 genome editing in a near-haploid human HAP1 cell line (HZGHC001314c006) (Horizon Discovery). The guide RNA 5′-AGCCAGTCCACGGACACTTC-3′ was used to induce a 5bp deletion

at the genomic site chr16:31182597, which is located in exon 3 of the FUS gene. The deletion results in a frameshift translation of 81 amino acids followed by a stop codon.

C. elegans

All *C. elegans* strains are on the N2 Bristol background and cultured at 20°C unless otherwise noted. Mutant strains obtained from the Caenorhabditis Genetics Center include RF54 *alg-1(gk214)X*, MT7626 *let-7(n2853)X*, OH812 *otIs114I*, and OH3646 *otIs114I; lsy-6(ot150)V*. The FX4439 *fust-1(tm4439)II* was received from the National Bioresource Project of Japan. All the mutant strains were backcrossed with the N2 strain at least four times. The strains generated by crossing in this study include IW480 *fust-1(tm4439)II;alg-1(gk214)X*, IW754 *fust-1(tm4439) II;let-7(n2853)X*, QK138/QK139 *otIs114[Plim-6::GFP]I;fust-1(tm4439)II*, QK136/QK137 *otIs114[Plim-6::GFP]I;fust-1(tm4439)II;lsy-6(ot150)*, IW755 *fust-1(tm4439)II;wIs54[Pscm::GFP]V*, IW756 *wIs54 [Pscm::GFP]V;alg-1(gk214)X*, and IW757 *fust-1(tm4439)II;wIs54[Pscm::GFP]V;alg-1(gk214)X*.

METHOD DETAILS

Mouse ES cell culture, motor neuron differentiation, and lentiviral transduction

Mouse ES cells were cultured and differentiated into motor neurons as described (McCreedy et al., 2014). The mouse ES cells were cultured in a gelatin-coated dish in medium containing DMEM (Life Technologies), 10% newborn calf serum, 10% fetal bovine serum, 10 μM thymidine, and 30 μM of each of the following nucleosides (Sigma): adenosine, cytosine, guanosine, and uridine. For differentiation, mouse ES cells were cultured in uncoated flasks with only DFK5 medium containing DMEM/F12 media with 5% knockout serum replacement (Life Technologies), insulin transferrin selenium (Life Technologies), 50 μM of nonessential amino acids (Life Technologies), 100 μM of BME, 5 μM of thymidine, and 15 μM of the following nucleosides: adenosine, cytosine, guanosine, and uridine. After 2 days, formed ES cell bodies were cultured in the DFK5 medium with 2 μM retinoic acid (Sigma) and 600 nM of SAG (Millipore) for 4 days, and the medium was changed every 2 days. Then, ES cell bodies were trypsinized and seeded in ornithine and laminin coated plates with DFK5 medium containing 5 ng/ml of glial-derived neurotrophic factor (GDNF; Peprotech), 5 ng/ml of neurotrophin-3 (NT-3; Peprotech), 5 ng/ml of brain-derived neurotrophic factor (BDNF; Peprotech), and 4 μg/ml of puromycin for a day. Next day, the medium was switched to modified DFKNB media containing half of DFK5 and half of Neurobasal media (Life Technologies), B27, 5 ng/ml of GDNF, 5 ng/ml of BDNF and 5 ng/ml of NT-3. The neurons were validated by immunostaining with Tuj1 (Cell signaling, TU-20).

Human FUS WT and R495X cDNAs were cloned into pLenti-CMV-Puro-Dest vector (Addgene). For transfection, 4 μg of psPAX2 and 0.5 μg of pMD2G and 5 μg of pLenti-CMV-Puro-FUS or pLenti-CMV-Puro-FUS R495X were transfected in a 10 cm dish of HEK293 cells with the large T antigen expression. After 2 days, the medium of transfected HEK293 cells was filtered through 0.45 μm membrane. The medium supernatant was centrifuged at 25,000 rpm X 90 min at 4°C in SW-41 rotor (Beckman). After centrifugation, the supernatant was discarded. 100 μL of PBS was added into the tube to dissolve pelleted virus. For transduction, 10 μL of virus and 4 μg/ml of polybrene were added into differentiated mouse motor neurons in 60 mm dishes.

Plasmid and antibody

The eGFP-PARP-13, eGFP-G3BP1, eGFP-AGO2, pRCP-6X and pRCP-0X constructs were described previously (Leung et al., 2011). The Pp-Mt-HDAC4 and Pp-WT-HDAC4 reporters were previously described (Williams et al., 2009). The V5-FUS constructs were previously described (Ito et al., 2011). The myc-tagged constructs, including FUS, R495X, R521C, and SOD1, were each subcloned in a modified mammalian expression vector, pRK5-myc, at the SalI site, downstream and in-frame with the myc epitope MEQKLISEEDL. The FUS shRNA construct was cloned by inserting small hairpin oligonucleotides targeting FUS coding sequence (TTGAGTCTGTGGCTGATTACTTCAAGCAG) into the pRFP-C-RS (Origene) using *BamHI/Hind*III restriction sites. The antibodies and their experimental conditions are listed in the Key Resources Table.

The pmirGLO Luciferase constructs containing the WT or mutant *ZEB1* 3′ UTR starting at nucleotide 4592 (NM_001174094.1) were generated by ordering and annealing oligos with PmeI and SbfI overhangs in NEB2 buffer (New England Biolabs). This region is designated as a non-coding portion of Exon 9 of *ZEB1*. Annealed oligos were cut and subcloned into pmirGLO Dual-Luciferase miRNA Target Expression Vector (E1330; Promega) via these restriction sites. Oligos are as shown below:

WT ZEB1 3′ UTR: (letters in bold denote restriction sites)
Sense (5′->3′)

1) **AAAC**GTAAGTGCCATTTCTCAGTATTTTCAAGGCTCTAACCCGCCTTCATCCAATGTGTG
2) GCCTACAATAACTAGCATTTGTTGATTTGTCTCTTGTATCAAAATTCCCAAATAAAACTTAAAACCACTGAC**CCTGCA**   (phosphorylated on 5′ end)

Anti-sense (5′->3′)

3) **GG**GTCAGTGGTTTTAAGTTTTATTTGGGAATTTTGATACAAGAGACAAATCAACAAATGCTAGTTATT
4) GTAGGCCACACATTGGATGAAGGCGGGTTAGAGCCTTGAAAATACTGAGAAATGGCACTTAC**GTTT** (phosphorylated on 5′ end)

ZEB1 3′ UTR with mutant miR-200c seed site
Replaced oligos 1) and 4) from above with: (letters underlined denote mutation)

1) **AAAC**GTAAGTGCCATTTCT<u>ACGAAC</u>TTTCAAGGCTCTAACCCGCCTTCATCCAATGTG
4) GTAGGCCACACATTGGATGAAGGCGGGTTAGAGCCTTGAAA<u>GTTCGT</u>AGAAATGGCACTTAC**GTTT**   (phosphorylated on 5′ end)

ZEB1 3′ UTR with mutant FUS binding site
Replaced oligos 2) and 3) from above with: (letters underlined denote mutation)

2) GCCTACAATAACTAGCATTTGTTGATTTGTCTCTTGTA<u>G</u>CAAAA<u>G</u>TCCCAAA<u>C</u>AAAACT<u>G</u>AAAACCACTGAC**CCTGCA**   (phosphorylated on 5′ end)
3) GGGTCAGTGGTTTT<u>C</u>AGTTTT<u>G</u>TTTGGG<u>C</u>ATTTTG<u>C</u>TACAAGAGACAAATCAACAAATGCTAGTTATT

The pmirGLO Luciferase constructs containing the WT or mutant *TXNIP* 3′ UTR were generated by annealing oligos with PmeI and SbfI overhangs in NEB2 buffer (New England Biolabs).

WT TXNIP 3′ UTR (letters in bold denote restriction sites)
TTTAAACAAAAGCCATTTTTGGAGCCTATTGCACTGTGTTCTCCTACTGCAAATATTTTCATATGGGAGGATGGTTTTCTCTTCATGTA
AGTCCTTGGAATTGATTCTAAGGTGATGTTCTTAGCACTTTAATTCCTGTCAAATTTTTTGTTCTCCCCTTCTGCCATCTTAAATGTAA
GC**CCTGCAGG**

TXNIP 3′ UTR with mutant miR-20b seed site (letters underlined denote mutation)
TTTAAACAAAAGCCATTTTTGGAGCCTATTGCACTGTGTTCTCCTACTGCAAAGAATGTCAAAAGGGAGGAAGGAGAGCTCTTCAT
GTAAGTCCTTGGAATTGATTCTAAGGTGATGTTCTT<u>ACCTCATA</u>AATTCCTGTCAAATTTTTTGTTCTCCCCTTCTGCCATCTTAAATG
TAAGC**CCTGCAGG**

TXNIP 3′ UTR with mutant FUS binding site (letters underlined denote mutation)
TTTAAACAAAAGCCATTT<u>A</u>AGGAGCCTAT<u>A</u>GCACA<u>G</u>GGTTCTCCTAC<u>G</u>GCAAATATTTTCATATGGGAGGATGGTTTTCTCTTCATG
<u>A</u>AAGTCCG<u>A</u>GGAATTGATTCTAAGG<u>A</u>GA<u>A</u>GTTCTTAGCACTTTAATTCC<u>A</u>GACAAAT<u>AT</u>AGA<u>G</u>ATCTCCCCTTC<u>A</u>GCCATCTTAAATG
TAAGC**CCTGCAGG**

Microarray and qPCR analysis
For microarray profiling experiments, 6×10^6 HEK293 cells (ATCC) were plated onto 100 mm plates prior to transfection with either myc-FUS or myc-R495X and pmax-GFP (Amaxa) as a marker with Lipofectamine 2000 (Life Technologies). After 24 hr, cells were trypsinized and resuspended in FACS (fluorescence-activated cell sorting) Buffer (1X PBS, 100 mM EDTA, 1% FBS) and sorted based on GFP fluorescence. RNA was immediately isolated from sorted cells using phenol-chloroform extraction with TRIzol reagent (Invitrogen) according to manufacturer's instructions. Half of the isolated RNA was then submitted for the Agilent microRNA microarray and the other half was further purified using QIAGEN's RNeasy Kit, which included an on-column DNase treatment, and then submitted for the Affymetrix Exon 1.0 microarray. Both Affymetrix Exon Array and Agilent MicroRNA Microarray data can be found at Gene Expression Omnibus repository (GEO: GSE68504).

For qPCR validation of mRNA microarray results, myc-FUS or myc-R495X was transfected to HEK293 cells using Lipofectamine 2000 (Life Technologies). After 24 hr, RNA was extracted using the miRNeasy Mini Kit (QIAGEN) and treated with the RNase-Free DNase Set (QIAGEN). RNA was reverse-transcribed using the HiFlex buffer with QIAGEN's miScript RT II kit and then the resultant cDNAs were amplified using QIAGEN's Quantitect SYBR Green PCR Kit using the Bio-Rad's MJ Mini Thermocycler or the CFX96 Real Time PCR Detection System (Bio-Rad). Fluorescence levels were detected and measured using the Bio-Rad CFX Manager software. Relative gene expression changes were calculated using the Pfaffl method with GAPDH as the reference gene. The qPCR primer sequences are listed in the Key Resources Table.

For qPCR validation of miRNA microarray results, RNA was reverse-transcribed and amplified similarly as mRNA except normalization was done against human snoRNA RNU6.2 (MS00033740, QIAGEN). Statistical analyses are based on delta Ct values using two-tailed, paired t test, $\alpha = 0.05$. To detect mature miRNAs, a specific primer assay against hsa-miR-200c (QIAGEN MS00003752) was used. To detect primary transcript forms of miR-200c, the Pri-miRNA assay Hs03303157_pri (4427012, Life Technologies) was employed and normalized with the TaqMan Gene Expression assay against TBP (Hs004271621_m1), using the TaqMan PCR Mastermix (4304437, Applied Biosystems).

Luciferase assay
For CXCR4 reporter assays, HEK293 cells were plated in 96-well plates 24 hr and transfected with 11.1 ng of pGL3 plasmid, 33.3 ng of pRCP-6X or pRCP-0X, 155.6ng GFP or myc-tagged constructs, and 10 nM siCXCR4 or control siRNA using 0.5 μL Lipofectamine 2000/3000 (Invitrogen). Alternatively, MEF or HAP1 cells were plated in 24-well plates and transfected with 20 ng of pGL3 plasmid, 120 ng of pRCP-6X or pRCP-0X, and 100 nM siCXCR4 or control siRNA using 1 μL Lipofectamine. For the FUS rescue experiments, 200 ng of FUS-V5 or LacZ-V5 plasmid were cotransfected into HAP1 cells, a dilution of the transfection mix that appeared to result in relatively lower sensitivity of the reporters. 24 hr after luciferase transfections, cells were washed with 1X PBS and then lysed in

1X Passive Lysis Buffer (Promega). The *Renilla* luciferase activity in each condition is normalized to the firefly luciferase activity of the pGL3 reporter. Luciferase activity is defined as fold repression, which is calculated by dividing the normalized luciferase activity in response to control All-Stars siRNA by the activity exerted by the CXCR4 siRNA.

For the HDAC4 reporter system, 10 nM of miR-206 (Dharmacon) was used in place of the CXCR4 siRNA, 11.1 ng of pRCP-0X in place of the pGL3 plasmid, and HDAC4 reporters in place of the CXCR4 constructs. The siRNA perfectly complementary to HDAC4 3′ UTR was synthesized at Dharmacon with the following sequence: sense (GGAAGGGAGCUGGGAGCAAUU) and antisense (UUGCUCCCAGCUCCCUUCCUU). Firefly luciferase activity was normalized to the *Renilla* luciferase activity and was defined as fold repression as described above. For the pmirGLO luciferase assays, 1.5×10^4 HEK293 cells were plated per well of a 96-well plate 24 hr prior to transfection. We transfected 0.5 ng pmirGLO luciferase reporter, 100 ng of pCMV-hsa-miR-200c/505 (Origene), and an empty pcDNA3.1 vector (Invitrogen) using 0.5 μL Lipofectamine 2000 (Invitrogen) for 48 hr, followed by 1X PBS wash and lysis in 1X Passive Lysis Buffer (Promega). Recombinant miR-200c, miR-20b, and negative control miRNAs (Dharmacon) were also used.

All luciferase samples were processed using the Dual Luciferase Reporter assay system (Promega) according to manufacturer's recommendations and read using a plate reader (Biotek Synergy H1 Hybrid Reader), which used the Gen5 2.0 Data Analysis Software program with the following setting: dispense 40 μL LARII, delay two seconds, read and then dispense 40 μL of Stop and Glo, and delay another two seconds and then read again. The Firefly luciferase signals were normalized by dividing by the *Renilla* luciferase signals.

Proteomics

AGO2 immunoprecipitations were performed from EGFP-AGO2 or HA-AGO2 stably expressing HeLa cells, with EGFP alone or HA-LacZ as a negative control, respectively. Cell lysates were subjected to immunoprecipitation using anti-GFP (3E6; Invitrogen) and protein G dynabeads or anti-HA Affinity Gel (E6779, Sigma) and the samples were reduced with DTT and cysteines carbamido-methylated with iodoacetamide before separation on a Novex 4%–12% Bis-Tris protein gel. Gel slices were excised and digested with trypsin and peptides desalted with a C18 StageTip before nano-scale liquid chromatography-mass spectrometry analyses using an Agilent 1100 HPLC and an LTQ-Orbitrap (Thermo, Bremen).

Protein and RNA co-immunoprecipitation and immunocytochemistry

The co-immunoprecipitation of endogenous AGO2 proteins with myc-FUS is adapted from a previously described protocol (Moser et al., 2009). One 15-cm dish of HEK293 cells was transfected with 10 μg myc-tagged FUS constructs for 24 hr. Protein A/G agarose beads (Pierce) were preconjugated with 10 μg of myc antibody (M4439, Sigma) or control mouse IgG overnight. The transfected cells were lysed in ice-cold NET2F buffer (50 mM Tris-HCl, pH 7.4, 150 mM NaCl, 2 mM EDTA, pH 8.0) except for the use of 0.3% NP-40, followed by sonication for 50 s twice using the Bioruptor UCD-200 (Diagenode). 3 mg of total protein was used for immunoprecipitation with 3.5-hr incubation, followed by western blotting analysis.

To perform co-immunoprecipitation with endogenous FUS from mouse brain, adult mouse forebrain was collected and immediately homogenized in cold lysis buffer with 2X protease inhibitor (Roche). Supernatant was then collected and precleared with protein A/G agarose beads (Pierce). Supernatants were split into two pairs: 1) and 2) were mixed with 5 μg of rabbit anti-FUS (Bethyl) or 5 μg of negative control for rabbit IgG and 3) and 4) had 5 μg of mouse anti-FUS (Santa Cruz) or 5 μL of negative control for mouse IgG. Tubes were rocked for 1.5 hr at 4°C and then mixed with beads for another 2 hr. After washing, samples were boiled in 2X Laemmli buffer and processed for immunoblotting.

To perform the co-immunoprecipitation of V5-FUS variants with AGO2, cells plated on 15-cm dishes were transfected with 10 μg of each V5-tagged FUS construct and then processed using the AGO2 immunoprecipitation protocol (see above), with the beads pre-conjugated to an AGO2 antibody (rat monoclonal, Clone HA9, SAB4200085, Sigma, and mouse monoclonal, Clone 2D4, 014-22023, Wako) or mouse IgG (control). 1.5 mg of protein was used for immunoprecipitation. To perform the co-immunoprecipitation of purified AGO2 and FUS proteins, human AGO2 protein was isolated in complex with copurified insect small RNAs using a published protocol (Elkayam et al., 2012) and GST-tagged human FUS protein was purified as previously described (Sun et al., 2011). AGO2 was pulled down with a rabbit antibody (Cell Signaling, C34C6); GST-FUS and a control GST was detected by a mouse-derived GST antibody (Santa Cruz, sc-138).

To perform RNA immunoprecipitation with proteins, following 24–48 hour transfection of HEK293 cells with myc-FUS, myc-R495X, myc-SOD1, or empty pcDNA3.1 (Invitrogen), and pCMV-miR-200c/miR-505 (Life Technologies) via Lipofectamine 2000, cells were lysed with polysome lysis buffer. A specific amount of total protein (1.5–3 mg) of total protein was used for immunoprecipitation with anti-myc conjugated agarose beads (Millipore). After immunoprecipitation, beads were treated with Proteinase K to release the proteins bound with RNAs, which were then isolated using Qiazol (QIAGEN). When FUS-V5 was transfected and immunoprecipitated by the anti-V5 antibody and Pierce protein A/G magnetic beads, a construct expressing LacZ-V5 was used as a control. The levels of microRNAs were normalized against that of the snoRNA RNU6.2, which was unchanged relative to total RNAs before or after the RIP. The inhibition of miR-200c was achieved by transfection of a specific antagomir known as miRIDIAN hairpin inhibitor against has-miR-200c-3p (Dharmacon, IH-300646-06-0002) as compared with a negative control (Dharmacon, IN-001005-01-05). The rabbit anti-FUS antibody (Bethyl) was used for the endogenous FUS RNA immunoprecipitation. For the AGO2 RNA immunoprecipitation, an AGO2 immunoprecipitation and miRNA isolation kit (Wako) was used on lysates from FUS WT or KO cells.

For the 2′-O-Me capture of miR-200c, a biotinylated 2′-O-methylated RNA oligonucleotide complementary to has-miR-200c-3p was synthesized and applied to cell lysates to pull down miR-200c through Streptavidin beads. Wild-type or FUS knocked

out HAP1 cells were collected and resuspended in ice-cold lysis buffer (25 mM HEPES-KOH PH 7.4, 120 mM NaCl, 1 mM EDTA, 2.5% glycerol, 0.5% Triton X-100, 2 mM Dithiothreitol, 1 × Protease Inhibitor Cocktail [Sigma], 0.2 U/μl RiboLock RNase Inhibitor [Thermo Scientific]) for 10 minutes. The lysates were spun at 17,000 × g for 15 min at 4°C and the supernatants were collected to determine protein concentrations. 50 μL of Dynabeads M-280 Streptavidin beads (Thermo Scientific) were prepared by three times of washing with binding and washing buffer (5 mM Tris-HCl PH 7.5, 1 M NaCl, 0.5 mM EDTA, 0.2 U/μl RiboLock RNase Inhibitor [Thermo Scientific]) and blocked with 1% BSA. The prepared beads were mixed with 100 pmol of biotinylated miR-200c complementary 2′-O-Methylated oligonucleotide in the binding and washing buffer by rotation. After incubation for 45 minutes at room temperature, the beads were washed three times with the lysis buffer and then 1.5 mg of protein lysate was added and incubated for 45 minutes. The supernatant was collected for RNA extraction by miRNeasy Mini Kit (QIAGEN), and the beads were washed three times with the lysis buffer and resuspended in Laemmli 1 × loading buffer with boiling for 5 minutes. The elutes were resolved on SDS-Polyacrylamide gel for western blotting. The miR-200c complementary 2′-O-methylated oligonucleotide was synthesized by Integrated DNA Technologies and its sequence is the following: /5BiosG/ mUmCmUmUmCmUmCmCmAmUmCmAmUmUmAmCmCmCmGmGmCmAmGmUmAmUmUmAmAmCmCmUmU.

To perform the immunocytochemistry of endogenous FUS and AGO2, HeLa cells plated on glass coverslips were fixed and stained with a mouse anti-AGO2 antibody (Wako) and a rabbit anti-FUS antibody (Bethyl), followed by secondary antibodies including anti-rabbit Alexa Fluor 488 and anti-mouse Alexa Fluor 555 (Invitrogen).

Electrophoretic mobility shift assay

Purified GST-FUS and GST-R495X were made as previously described (Sun et al., 2011). Standard binding reactions are 10 μL in total and consist of a final concentration of 10 mM Tris, pH 8.0, 25 mM KCl, 10 mM NaCl, 1 mM MgCl$_2$, 1 mM DTT, 0.1 mg/ml acetylated BSA, 2 nM RNA probe, 0.1 mg/ml yeast tRNA (Sigma), 0.4 U/μl RiboLock RNase Inhibitor (Thermo Scientific), which were incubated at room temperature for 30 minutes prior to loading with 2 μL of 50% glycerol. For competition assays, the reactions were the same as above except for the addition of unlabeled miR-200c. All gel shifts were run on 6% native polyacrylamide gels (Acrylamide/Bis 37.5:1) in 0.5X TBE buffer and run on 150 V for 0.5 hours. All gel shifts for Figure 6 were captured with Amersham Typhoon Imager 9200 and analyzed with ImageQuant version 5.2.

RNA Probes *(synthesized by* Integrated DNA Technologies*)*

GGUG oligo: UUGUAUUUUGAGCUAGUUUGGUGAC-Cy3
MiR-200c (untagged): UAAUACUGCCGGGUAAUGAUGGA
MiR-200c: UAAUACUGCCGGGUAAUGAUGGA-Cy5
MiR-505: CGUCAACACUUGCUGGUUUCCU-Cy5

Single molecule binding assay

FUS protein with a N-terminal His tag was expressed from a construct (kindly provided by Jacob Schwartz and Nicolas Fawzi) in *E. coli* [BL21(DE3)], purified to homogeneity as a monomer via Ni Affinity (HisTRAP HP) followed by size exclusion chromatography, and stored in a buffer containing 1 M KCl and 1 M urea to prevent aggregation. For the single molecule binding assay, FUS protein was immobilized on the surface of a PEG-coated quartz slide using biotinylated anti-His antibodies. The surface of the PEG slide was treated with 0.05 mg/ml Neutravidin for 3 min and then treated with 1:100 dilution of the biotinylated antibody diluted in T50 (10 mM Tris-HCl pH 7.5 and 50 mM NaCl). A solution of 200 nM protein in 100 mM KCl and 20 mM Tris-HCl pH 7.5 was added to the antibody-coated surface for 15 min to immobilize FUS proteins. To test the binding affinity, cy5-labeled miRNAs of a concentration gradient were added onto the surface and incubated for 15 min before washing with a buffer containing 100 mM KCl, 20 mM Tris-HCl pH 7.5, and an oxygen scavenging system (0.5% glucose, 1 mg/mL glucose oxidase, and 88 U/mL catalase in 10 mM Trolox). Measurements were performed by a home-built total internal reflective fluorescent (TIRF) microscope using an EMCCD Andor camera. Quantifications were done by measuring the number of individual fluorescent spots in multiple imaging field of views for each condition.

C. elegans

For the *C. elegans* heterochronic phenotype analysis, L4 worms were selected and cultured at the designated temperatures. The worms were scored for the lateral alae formation 16 hours after L4. The seam cells on both sides of the body were quantified at the L4 stage. The *alg-1* worms were scored for the vulva bursting or the worm bag phenotypes 3 days after L4 at 20°C. For the *let-7* heterochronic phenotype analysis at 25°C, worms were synchronized by egg laying for 2 hours, and 48 hours later scored for the vulva bursting during the L4 stage. For the *lsy-6* ASEL specification assay, synchronized populations, attained by plating synchronized L1s, were generated by alkaline-hypochlorite embryo extraction and overnight hatching in M9. ASE neuron misspecification was scored in adults at 20°C using *otIs114[Plim-6::GFP]* to indicate ASEL.

Bioinformatic analysis

To obtain 3′ UTR sequence lengths for all genes present in our Affymetrix Exon 1.0 microarray, we downloaded the human genome (hg19) from the University of California, Santa Cruz (UCSC) Genome Browser. We used the RefSeq transcript IDs for the analysis, such that genes with more than one unique RefSeq would be counted more than once. For the analysis on the 3′ UTR lengths of

AGO- and FUS-binding targets, we used previously reported CLIP data (Hafner et al., 2010; Hoell et al., 2011) from HEK293 cells that was deposited in an RNA-protein interaction database, doRiNA (Blin et al., 2015). For detailed analysis of RNA-binding sites of different proteins, we processed CLIP raw sequencing data and identified T-to-C mutations as crosslinked sites from a collection of previous datasets from HEK293 cells, including FUS (Hoell et al., 2011), TNRC6A (Hafner et al., 2010), AGO2 (GEO: GSE28865), FMR1 and FXR1 (GEO: GSE39686), AUF1 (GEO: GSE52977), and NOP56 (GEO: GSE43666). Adaptor sequence (TCGTATGCCGTCTTCTGCTTG) was removed from the sequencing data using fastx_clipper from FASTX toolkit (http:// hannonlab.cshl.edu/fastx_toolkit/index.html), and only the clipped reads with a minimum length of 15 bases were kept. Clipped reads were aligned to the human genome using bowtie v1.1.2 with standard parameters and a pre-built hg38 index. Aligned reads were subsequently processed using samtools v0.1.19, and mutations or variants were identified using samtools mpileup using the option -Buf. Mutations with total minimum read depth of five were used for further analysis. The effect of the mutations to the human genes was analyzed using snpEff v4.1 by examining only the canonical transcripts as determined by the snpEff team based on the UCSC hg38 annotation. Details of the canonical transcripts based on hg38 annotation were extracted from snpEff using the dump command for further annotation (e.g., java -Xmn4g -jar snpEff.jar dump -v -canon -txt hg38 > hg38.txt). T-to-C mutations that are associated with canonical transcripts on the appropriate strands were identified and organized using custom scripts written in R. T-to-C mutations (or A-to-G mutations in the complementary strand) indicate the RNA-protein binding sites because this specific mutation occurs as a result of UV crosslinking of RNA to RNA-binding protein in PAR-CLIP (Hafner et al., 2010). If a T-to-C mutation was found to be associated with single genomic location but associated with multiple gene names, the conflicts were resolved so that each T-to-C mutation is associated with a single gene name. In the cases where the 3′ UTR of a gene contains one or more T-to-C mutations associated with two different RNA-binding proteins, the minimum distance between the T-to-C mutations associated with each RNA-binding protein was calculated using additional custom R scripts. The transcript targets of various human miRNAs were analyzed by the *IPA* (Ingenuity Pathway Analysis) software under the miRNA target filter. The analysis for the direction of changes in the miRNA-targeted mRNAs was run using Partek Genomics Suite v6.6.

To select non- or low-expressing miRNAs as negative controls, we analyzed the miRNA expression profiles from the miRmine database (Panwar et al., 2017) and our own microarray experiments. A high-quality miRNA-seq dataset GEO: GSE56836 was analyzed for HEK293T cells. All miRNA reads were normalized and counted as reads per million (RPM). MiRNAs with RPM < 1 were designated as non- or low-expressing miRNAs, including miR-584, miR-4257, miR-429, and miR-3153. In our own miRNA microarray experiments, miR-584 was not probed and miR-4257, miR-429, and miR-3153 were all low-expressing miRNAs (Table S3). The experimentally validated target transcripts were then identified as *SETD5* (miR-584), *ZNF473* (miR-4257), *WASF3* (miR-429), *RGMB* (miR-3153), and *TMBIM6* (miR-3153).

QUANTIFICATION AND STATISTICAL ANALYSIS

Statistical analysis

For all RNA immunoprecipitations, RNA enrichment is calculated by subtracting the delta Ct value of the input and the $\log_2$ value of the input dilution factor from the delta Ct value of each RNA pull-down. t tests or ANOVAs were then run on these raw Ct values. Analyses for luciferase assays are described under those sections. Analyses on qPCR microarray confirmations are conducted on raw Ct values. Statistical tests were performed using degrees of freedom dependent on homogeneity of group variance. The sample size n represents biological replicates. A summary of the statistical analyses is shown in Table S5.

DATA AND SOFTWARE AVAILABILITY

Data Resources

The accession number for the Affymetrix Exon Array and Agilent MicroRNA Microarray data deposited in Gene Expression Omnibus repository is GEO: GSE68504.